N O T I C E

THIS DOCUMENT HAS BEEN REPRODUCED FROM MICROFICHE. ALTHOUGH IT IS RECOGNIZED THAT CERTAIN PORTIONS ARE ILLEGIBLE, IT IS BEING RELEASED IN THE INTEREST OF MAKING AVAILABLE AS MUCH INFORMATION AS POSSIBLE

Two-Stage Combustion for Reducing Pollutant Emissions From Gas Turbine Combustors

Richard M. Clayton
David H. Lewis

February 1, 1981

PREFACE

The work described in this report was performed by the Control and
Energy Conversion Division of the Jet Propulsion Laboratory and was
supported by NASA/OAST, Research and Technology Division.

ACKNOWLEDGMENT

ABSTRACT

A two-stage gas turbine combustor concept employing a very fuel-rich partial oxidation first stage has been explored for broadening the combustion margin between ultralow emissions and the lean stability limit. Combustion and emission results are presented for a premix combustor fueled with admixtures of JP5 with neat H_2 and of JP5 with simulated partial-oxidation product gas. The combustor was operated with inlet-air state conditions typical of cruise power for high performance aviation engines. Ultralow NO_x, CO and HC emissions and extended lean burning limits were achieved simultaneously.

Laboratory scale studies of the non-catalyzed rich-burning characteristics of several paraffin-series hydrocarbon fuels and of JP5 showed sooting limits at equivalence ratios of about 2.0 and that in order to achieve very rich sootless burning it is necessary to premix the reactants thoroughly and to use high levels of air preheat.

The application of two-stage combustion for the reduction of fuel NO_x is reviewed.

An experimental combustor designed and constructed for two-stage combustion experiments is described but was not operated.

iv

CONTENTS

Figures

Tables

SECTION I

INTRODUCTION

New combustor design concepts relative to those used in contemporary aviation engines will have to be developed if the emission of gaseous pollutants from future engines is to be minimized (Refs. 1-3). This prognosis results primarily from the difficulties associated with minimizing the oxides of nitrogen emissions (NO_x), though the actual excursion from present design practice will be governed by the degree of NO_x control required by eventual governmental regulations. Current standards proposed by the Environmental Protection Agency for the control of air pollution from aircraft and aircraft engines are contained in the Federal Register, Vol. 43, No. 58, March 24, 1978. The emissions of carbon monoxide (CO) and unburned hydrocarbons (HC) are generally easier to control but will also require substantial reductions simultaneously with the NO_x reductions. This simultaneous reduction is a complicating factor since combustor design considerations for low NO_x and low CO emissions are generally contrary to each other.

A very effective approach for controlling the formation of thermally generated NO_x is to incorporate fuel-lean burning in the primary heat release zone of the combustor in order to reduce peak flame temperatures. The emission of thermal NO_x, which is very temperature-dependent, can thus be dramatically reduced. However, the leanness required to achieve minimized NO_x emissions from a practical combustor leaves a relatively small lean-blowout margin. Furthermore, as the lean-blowout condition is approached, combustion becomes less stable and emission of CO and HC tend to increase rapidly.

Thus, the simultaneous minimization of all three pollutants via lean burning occurs over a very narrow range of mixture strength that is also close to the stability limit. Control of the local reacting mixture ratio is therefore crucial. This requirement and the necessity of providing for flame stabilization dictates that lean-burning combustor concepts must integrate premixing and flameholding schemes that are far removed from conventional combustor design practices.

A two-stage combustor concept that could broaden the combustion margin between ultralow emissions and the stability limit has been explored at JPL (Refs. 4-8). This concept would employ a very fuel-rich precombustion stage where a large portion of the fuel to the engine would be reacted with a small portion of the air to the engine, producing a fuel-gas stream ideally composed of more than 20% by volume of H_2 and CO, the remainder consisting mostly of N_2. This "fuel gas" exhibits combustion characteristics superior to those of raw hydrocarbon fuel by virtue of (a) its H_2 content, providing a reduced lean flammability limit, and (b) its hot, fully gaseous state, providing the potential for increased mixing and combustion rates, as well as reduced thermal radiation to the combustor walls. Moreover, experimental results reported in Ref. 9 suggest the potential of well-premixed, very fuel-rich reactions (equivalence ratio > 2) for suppressing the formation of intermediate

nitrogen compounds that are involved in the formation of NO from fuel-bound nitrogen. Thus, processing a substantial portion of fuel through a precombustion stage may also inhibit the production of fuel-generated NO_x in the final combustion stage.

The purpose of this report is to document the JPL work that has been accomplished since Ref. 4 was published. The main text of the report covers: (1) the final results of experiments using neat H_2/JP5 fuel mixtures, (2) the final results of experiments using a simulated partial oxidation product gas with JP5 fuel, and (3) the final results of laboratory burner experiments on fuel-rich combustion. A discussion of the application of two-stage combustion to the reduction of fuel NO_x, and a description of a two-stage combustor constructed to carry out combustion experiments, but which has not been operated, are included as Appendixes A and B, respectively.

Except for the laboratory experiments on fuel-rich burning at atmospheric pressure, all the combustion experiments were carried out with inlet-air state conditions typical for 30:1 compression ratio, high bypass, turbofan commercial aviation engines. The cruise condition of 1.18 MPa (11.6 atm) and 728 K (850°F) was emphasized, but some data was obtained at the take-off condition of 3.04 MPa (30 atm) and 811 K (1000°F).[1] A premix research combustor was used for all the high pressure experiments.

---

[1]Although SI units are used in this report, the principal measurements and calculations were made in English system units.

SECTION II

THEORETICAL CONSIDERATIONS

A.   PARTIAL-OXIDATION PRODUCTS

Although the partial-oxidation process can be carried out either
thermally or catalytically, the adiabatic, equilibrium composition of
the product gases are identical for the same initial reaction condi-
tions. Details of the paths of the combustion chemistry for either
reaction scheme are complex and not fully understood and their discus-
sion is beyond the scope of this report. Suffice it to say that the
overall process occurs with an excess of fuel and that the consumption
of the available oxygen by a portion of the fuel provides heat, CO_2, and
H_2O that react with the remainder of the fuel to produce a final product
gas whose composition is a function of the particular fuel stock and the
reaction mixture ratio.

Figure 1 shows the results of one-dimensional, equilibrium-
thermochemical calculations giving product composition (molar basis) and
temperatures for a typical conventional turbine fuel with a hydrogen-
to-carbon ratio of 1.92, over a range of fuel-rich air-to-fuel ratios
and at an operating condition in the range of interest to the present
work (nitrogen concentrations are not shown). The calculations were
made using the computer program described in Ref. 10.

Note that solid carbon (C_S) is predicted with A/F ratios less than
about 5.2 and that the product gas temperature increases rapidly at A/F
ratios greater than 5.2. Carbon monoxide, one of the two major combus-
tibles in the product gas, reaches a peak at about this A/F ratio,
whereas the other major combustible, H_2, shows an increasing volumetric
concentration in the A/F region of C_S formation. However, in terms of
the mass of H_2 produced per unit mass of hydrocarbon fuel, it can be
shown that H_2 mass productivity of the fuel also peaks at about the A/F
ratio of 5.2, as illustrated in Fig. 2.

Thus, from a theoretical standpoint, the optimal A/F ratio for
sootless H_2 production is about 5.2 (equivalence ratio 2.83) where the
H_2 content of the product gas is about 6% of the mass of the combus-
tibles in the gas. Based on the "actual product gas" shown in the right
hand side of Table 1 and the procedure outlined in Ref. 11, the lean
flammability limit (at ambient temperature) of this gas mixture with air
is estimated to occur at an overall A/F ratio of about 57 (includes the
air used to generate the product gas). This substantially reduced lean
limit compares to about 24 for turbine fuels. That reduction is the
central argument for the staged concept discussed herein.

B.   INTEGRATED COMBUSTION SYSTEM

Assuming that the technology for providing an optimized partial-
oxidation reactor existed, integrating it into a two-stage combustion
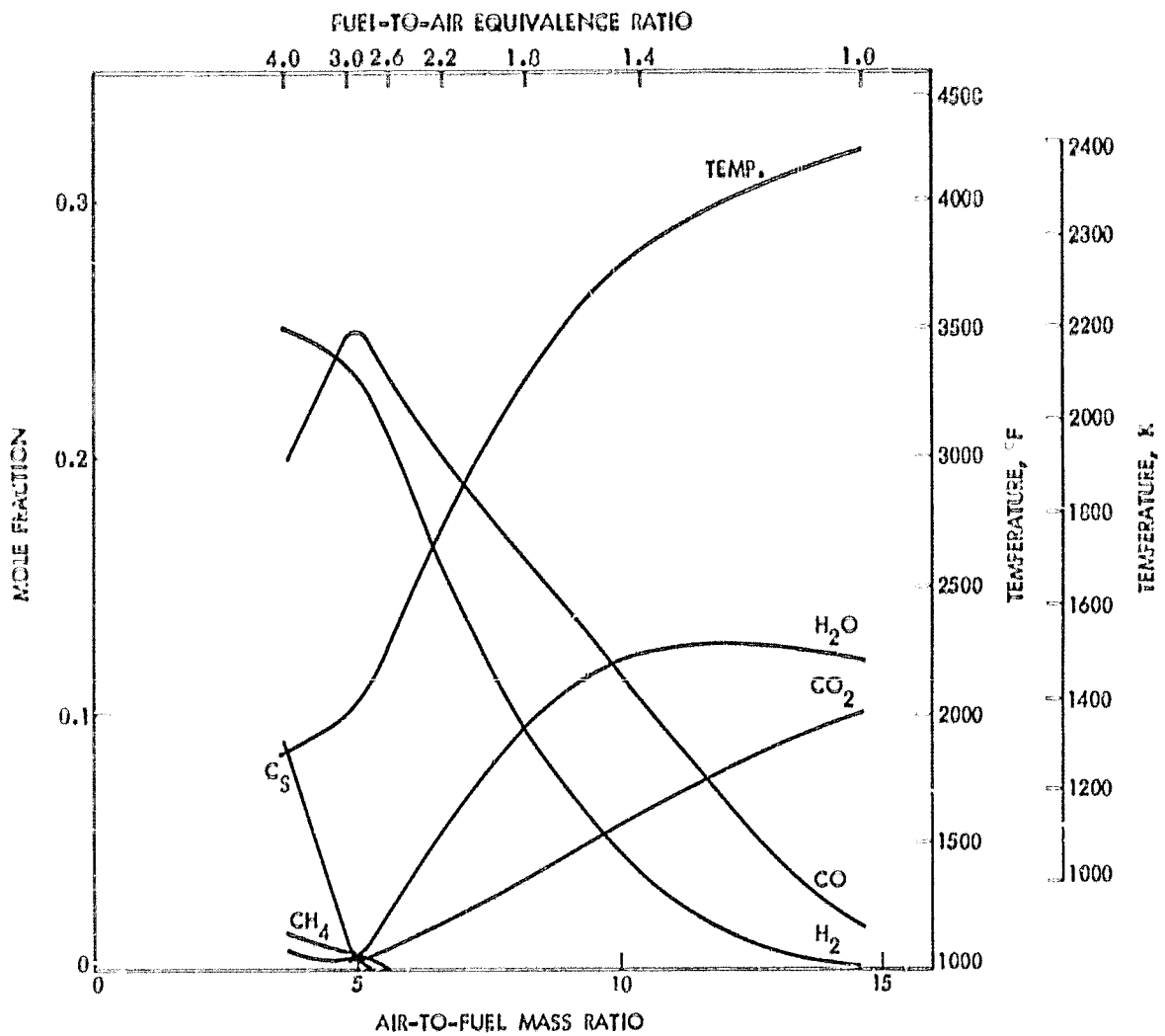
Figure 1. Theoretical equilibrium composition and temperature of fuel-rich products for inlet air at 778 K (940°F) and 2.53 MPa (25 atm); fuel H/C = 1.92
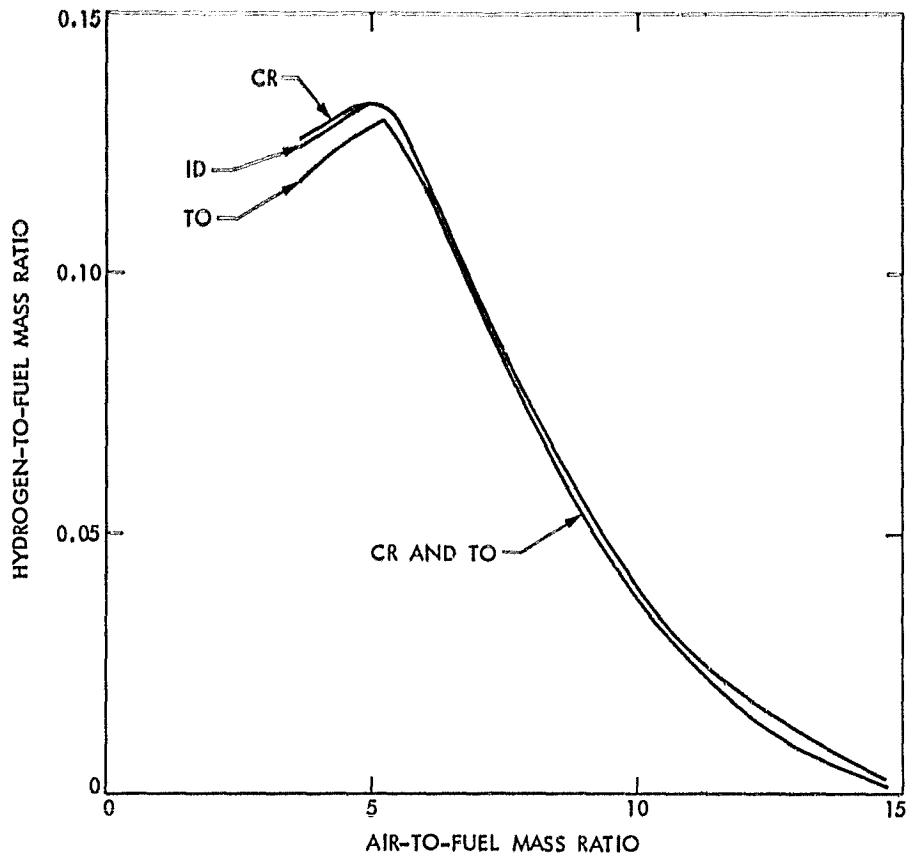
Figure 2. Theoretical hydrogen-to-fuel mass ratio for various inlet-air conditions typical for gas turbines: (TO) 778 K (940°F), 2.53 MPa (25 atm); CR 717 K (830°F), 0.81 MPa (8 atm); (ID) 422 K (300°F), 0.30 MPa (3 atm); fuel H/C = 1.92.
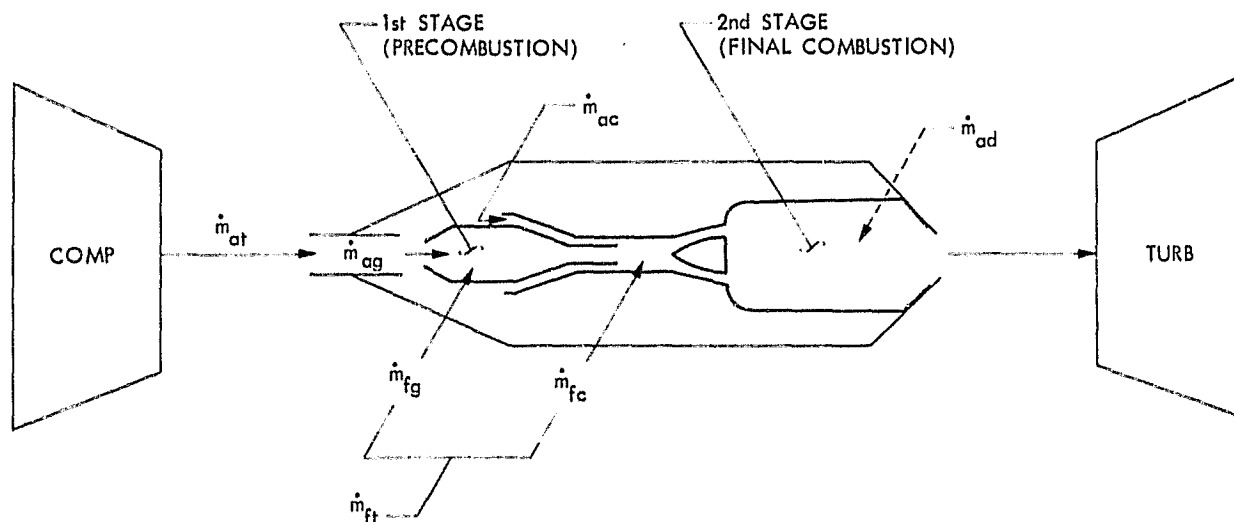
Figure 3. Schematic of integrated two-stage combustor.

2-3

Table 1. Gas composition.

Species/Miscellaneous Properties	Simulant Mixture		Actual Product Gas[a]	
	% Vol.	% Mass	% Vol.	% Mass
H_2	22.74	2.05	22.70	2.05
CO	24.94	31.66	24.70	31.37
CH_4	0.00	0.00	0.40	0.29
N_2	52.32	66.29	50.90	64.04
CO_2	0.00	0.00	0.50	1.00
H_2O	0.00	0.00	0.80	0.65
Combined Mol. Wt.	22.10		22.05	
Temperature	Ambient		1422 K (2100°F)	
H_2 in Total Combustibles	6.08% Mass		6.08% Mass	

[a] Equilibrium composition for fuel-air reaction products assuming 2.5 MPa (25 atm), 778 K (940°F) inlet air; fuel H/C = 1.92; and equivalence ratio = 2.83.

system has a substantial impact on present combustor design practices. A rudimentary conceptual design analysis serves to outline projected operational requirements and identifies potential design options that could accommodate the broad combustion range needed for aviation gas turbine engines.

An integrated two-stage system is depicted schematically in Fig. 3, where the various fuel and air flows are also identified. From the usual definition of equivalence ratio (ϕ) and the notation in Fig. 3, ϕ for the first stage is

$$\phi_g = \frac{\dot{m}_{fg}}{\dot{m}_{ag} R_s} \tag{1}$$

and ϕ for the second stage is

$$\phi_0 = \frac{\dot{m}_{ft}}{\dot{m}_{at} R_s} \tag{2}$$

where R_s is the stoichiometric fuel-to-air ratio for turbine fuel (taken as 0.068 throughout this report).

From Eqs. (1) and (2) it is easily shown that

$$\phi_0 = \phi_g \frac{S_a}{S_f} \tag{3}$$

where $S_a = \dot{m}_{ag}/\dot{m}_{at}$ and $S_f = \dot{m}_{fg}/\dot{m}_{ft}$ are the fractions of total air and total fuel, respectively, that are directed through the first stage; i.e., the air-and fuel-split ratios.

When the cooling-dilution air flow ($\dot{m}_{ad}$) is zero and all of the reactants are premixed prior to final combustion, the second stage equivalence ratio (ϕ_0) is not only the overall equivalence ratio for the system but is also the equivalence ratio for the final combustion reaction (ϕ_c). However, for $\dot{m}_{ad}/0$,

$$\phi_c = \frac{\phi_0}{1-X} \tag{4}$$

where $X = \dot{m}_{ad}/\dot{m}_{at}$. Thus, from Eqs. (3) and (4)

$$\phi_c = \frac{\phi_g S_a}{(1-X) S_f} \tag{5}$$

A conceptual operating map for a two-stage combustor can be constructed from Eq. (3) if the variation in the lean-flammability limit as a function of fuel-split ratio is also evaluated. It is assumed that the precombustion stage is operated at a constant equivalence ratio; therefore the product gas stream has a fixed composition and a fixed lean limit, such as mentioned previously. Admixtures of this composite fuel gas and supplemental raw-fuel vapor will have different lean limits in accordance with the Le Chatelier relationship outlined in Ref. 11. Thus, when all the raw fuel is processed through the first stage, the product gas is the only "fuel" burned in the second stage; therefore, the system lean flammability limit is at its minimum value. But when lesser amounts of raw fuel are processed (fuel split ratios < 1.0), the system lean limit increases by virtue of the richer limit of the raw fuel that bypasses the first stage and enters the combustion process in the second stage without prior processing.

The variation in the lean limit equivalence ratio (ϕ_{cL}) as a function of the fuel split ratio (S_f) is derived in Appendix C and can be expressed as

$$\phi_{cL} = \frac{\alpha_L R_g}{R_s \{R_g + S_f[1 + \alpha_L + \beta_L(1 + R_g)]\}} \tag{6}$$

where $R_g = \dot{m}_{fg}/\dot{m}_{ag}$; α_L is the fuel-to-air ratio at the lean limit for turbine fuel (taken as 0.0414 in this report); and β_L is a constant based on the lean limit of the first stage product gas relative to the lean limit of the turbine fuel (β_L estimated to be -0.6533 for $\phi_g = 2.83$).

Evaluations of Eqs. (3) and (6) are plotted in Fig. 4 for a constant $\phi_g = 2.83$, the theoretical optimum for sootless hydrogen yield. The solid curves represent Eq. (3) for three arbitrarily selected constant values of air split ($S_a = 0.05$, 0.10 and 0.15). Each of these lines also represents a constant total flow through the precombustion stage for particular engine power levels (i.e., particular total air flows to the combustion system). The dashed curve represents Eq. (6). This lean-limit line is a theoretical combustion limit, but not necessarily a lean blowout limit, since blowout is also a function of flame stabilization technique and reactant premixedness. Nevertheless, all other combustor factors fixed, fuels or fuel mixes with substantially lower flammability limits can be expected to provide substantially leaner blowout limits.

If all the system fuel is directed through the first stage, then operation of the combustion system lies along the horizontal at $S_f = 1.0$ on Fig. 4 and the air split would have to vary linearly with overall equivalence ratio in accordance with Eq. (3) with ϕ_g fixed and S_f set to 1.0. The control of the air split would probably require a so-called variable geometry combustor design.
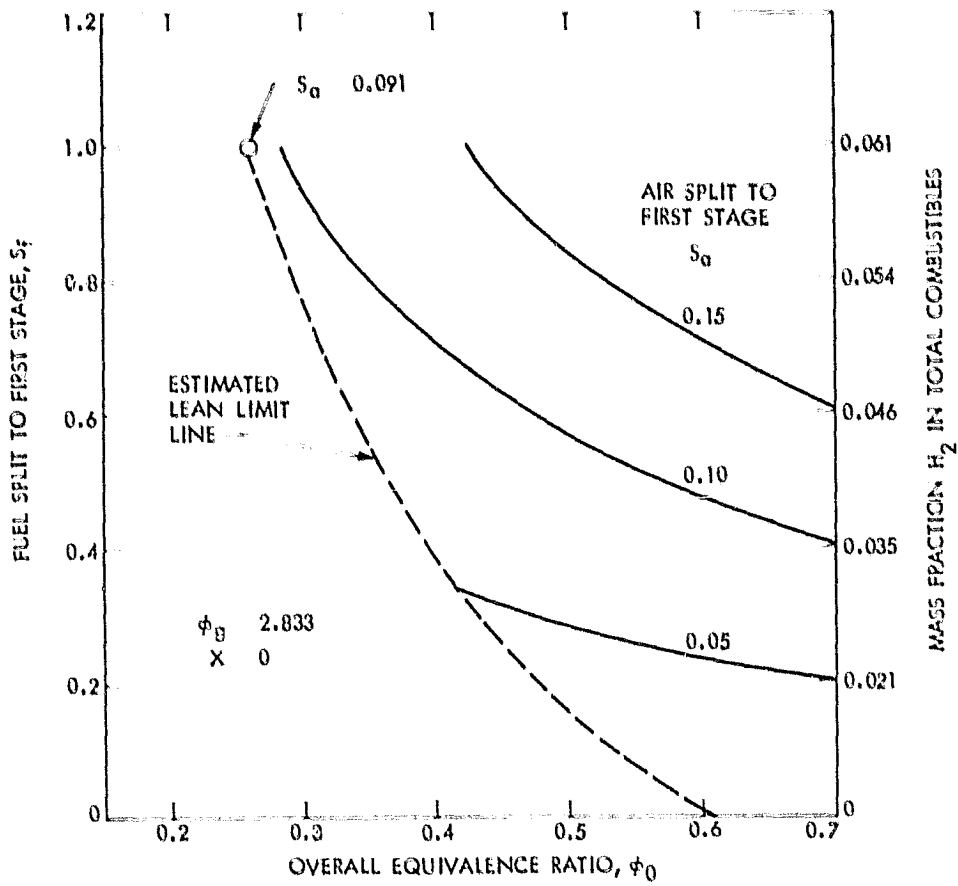
Figure 4. Conceptual operating map for two-stage combustion system.

If the final combustion is to be carried out totally premixed with all the air to the second stage ($\dot{m}_{ad} = 0$), then only the system equivalence ratio region to the right of the limit line, shown in Fig. 4, is theoretically viable for completing the combustion reaction started in the precombustion stage. If a portion of the total air flow is to be used for film-cooling and dilution ($\dot{m}_{ad} > 0$) as would be required for an engine combustor, the final combustion reaction would necessarily be richer, as shown by Eq. (4), and the overall equivalence ratio could lie to the left of the limit line so long as the final reaction equivalence ratio was to the right of the limit line. The final reaction equivalence ratio in that case depends on the fraction of the total system air used for cooling and dilution (X) and the over-all equivalence ratio required for a particular engine operating condition. An evaluation of Eq. (4) for this relationship is shown in Fig. 5 for overall equivalence ratios of 0.34, 0.31 and 0.16, which are typical for maximum, cruise, and idle power, respectively. Two different lean limits taken from Fig. 4 are also shown on Fig. 5. The lower value corresponds to levels of first stage throughput where $S_a \geq 0.091$ and the higher value corresponds to an arbitrarily selected low level of throughput with $S_a = 0.05$. In addition, NO_x limits are shown that correspond to the theoretical ϕ_c for each power level that would constrain kinetically controlled thermal NO_x (NO_2 basis) to the target emission index value of 1.0 g NO_2/kg fuel. These estimates were made using kinetics calculations outlined Refs. 4 and 5 for a dwell time of 2 ms.

Thus, for $S_a \geq 0.091$ Fig. 5 shows that a fixed air fraction of about 0.38 for cooling-dilution would keep the final reaction equivalence ratio (ϕ_c) above the lean limit and the NO_x below the target emission level for all power conditions. On the other hand, reduced first stage throughputs result in values of ϕ_{cL} that require amounts of cooling-dilution fraction that, if fixed, would be excessive for NO_x control at the higher power levels; for example, X = 0.62 with $S_a = 0.05$.

From the foregoing discussion and a further inspection of Figs. 4 and 5, four distinct schemes for system operation can be defined and are shown in Table 2. Scheme (1) would provide the greatest enhancement of lean-burning combustion margin. But scheme (2) might also be used if processing only a portion of it would be adequate. Scheme (2) would be simpler to implement because a variable fuel-split control is probably easier than a variable air split control, although compressor bleed might also be needed at low power to throttle system air mass flow while maintaining combustion stability. An optimized system which would require minimal variable geometry or compressor bleed control would utilize a first stage throughput corresponding to $S_a = \sim 0.10$.
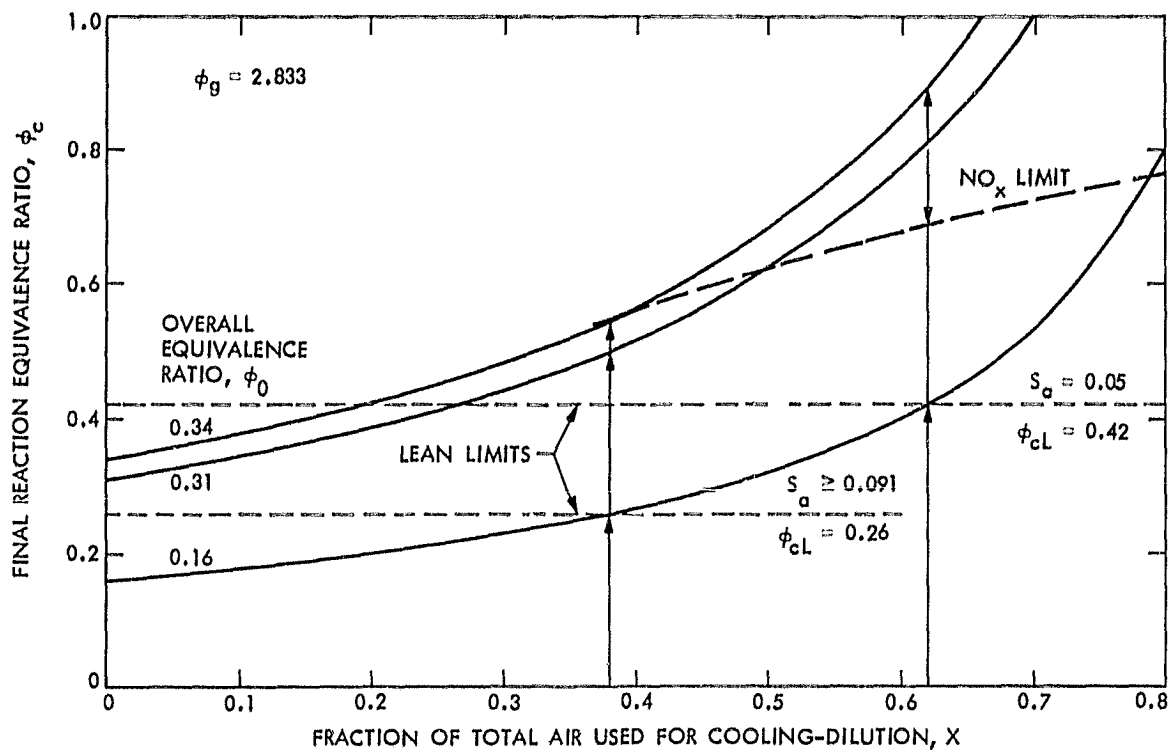
Figure 5. Variation of final reaction equivalence ratio with air used for cooling and dilution.

Table 2. Comparison of two-stage operational schemes.

	Operational Scheme	Air Split	Fuel Split	Advantage
1.	All fuel through first stage	Variable	Constant @ 100%	Greatest lean-burning enhancement
2.	Constant air split to first stage	Constant	Variable	Simpler control
3.	Parallel the lean limit line	Variable	Variable	None
4.	Constant fuel split to first stage (< 100%)	Variable	Constant	None

SECTION III

EXPERIMENTAL VERIFICATION

A.   HYDROGEN ENRICHMENT

1.   Description of Experiments

It was deemed important to establish the basic benefits of H_2 enrichment as the first step in the overall process of experimentally verifying the utility of the two-stage combustion concept.[2] The rationale for expecting the significant combustion enhancement with admixtures of H_2 and jet fuel is described in Refs. 4 and 5 along with interim experimental results. These results showed that the targeted ultralow emission levels could be achieved simultaneously, but that the proportion of H_2 required (10-12 mass % in the total fuel) was greater than the maximum theoretically available from a partial oxidation precombustion stage ($\sim 6\%$).[3] It was concluded from those results that improved premixing (H_2, jet fuel, and air) was necessary to decrease the H_2 requirement.

Subsequent modifications to the JPL MOD 2 burner resulted in the version shown in Figs. 6 and 7 described below. Pertinent design parameters are summarized in Table 3. Although the burner was not intended to be a scale version of the G. E. CF6-50 combustor, analogous design parameters for a production version are shown for reference. The experimental burner has about 4% of the mass throughput and about 40% of the combustion space rate of the engine combustor.

For testing, the burner is housed within a heavy-walled pressure vessel which also serves as a plenum chamber for a preheated inlet-air supply. (See Ref. 5 for a description of the test facility.) The burner is designed to utilize 100% of the air flow in the combustion process; thus air film cooling and air dilution, which are normally used in an engine combustor, are omitted. In this way, combustion effects from air injection are avoided during concept evaluation. The cylindrical combustion chamber is water-cooled, as are the inlet/flameholder assembly, sonic exhaust nozzle, and gas sample probe.[4]

The burner is intended to operate with a near-homogeneous fuel/air mixture. Premixing is accomplished in the mixing duct. The interfacial component between the combustion and premixing zones is an axisymmetric, combination step/bluff-body flameholder. A torch igniter provides ignition but is inactive once steady burning is obtained.

---

[2]Hydrogen enrichment of jet fuel can be considered to be a combustion enhancement scheme distinct from the two-stage combustion concept if the H_2 is available as a second fuel.

[3]It was expected that a similar H_2 proportion of the total combustibles would be required to achieve similar suppression of flammability limits regardless of the proportion of CO and jet fuel, since CO and jet fuel have similar lean flammability limits on an equivalence ratio basis.

AIR PLENUM HIGH PRESSURE
HOUSING, 48.3 (19.0) DIA

DETACHABLE PLENUM
END-DOME

AIR INLET AND
FUEL INJECTOR

WATER-COOLED
GAS SAMPLE
PROBE

H₂ OR
SIMULATED
PRODUCT
GAS

AIR

JP

AIR

10.2 (4.0)   12.2 (4.8)   25.4 (10.0)   5.1 (2.0)

WATER-COOLED
EXHAUST
NOZZLE

MIXING DUCT 5.3 (2.1) DIA

TORCH IGNITER

WATER-COOLED
COMBUSTION
CHAMBER 15.2 (6.0) DIA

DIMENSIONS IN CENTIMETERS (INCHES)

WATER-COOLED
INLET AND FLAME HOLDER

Figure 6.   MOD 2M research combustor installed in burner
housing.
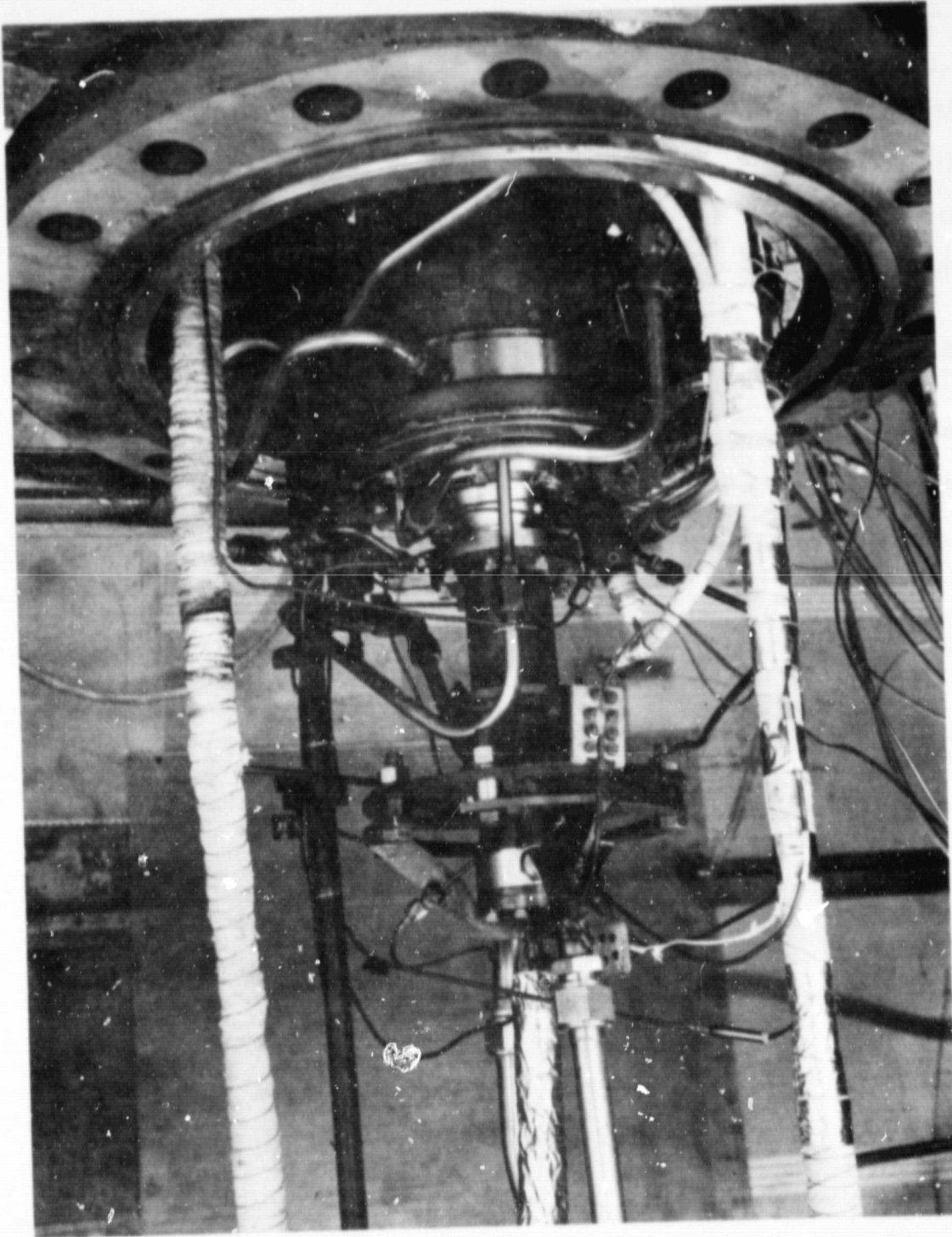
Figure 7. Photographic view of MOD 2M combustor with burner-housing flange open.

Table 3. JPL Mod 2M combustor design conditions and comparison with typical production engine burner.[a]

Specification item	Mod 2 burner[b]	Engine burner[b]
Air total pressure	3.04 MPa (30 atm)	3.04 MPa (30 atm)
Air total temperature	811 K (1460 R)	821 K (1477 R)
Air flow rate	4.5 kg/s (9.8 lbm/s)	103.4 kg/s (228 lbm/s)
Chamber reference velocity	18.3 m/s (60 ft/s)	25.9 m/s (85 ft/s)
Chamber dwell time (no recirculation)	5.0 ms	2.6 ms
Chamber L/D (shape)	1.7 (cylindrical)	3.0 (annular)
Combustion length	30.5 cm (12.0 in.)	34.8 cm (13.7 in.)
Combustion space rate[c]	0.88×10^6 J/hr-m^3-N/m^2 (2.4×10^6 Btu/hr-ft^3-atm)	2.2×10^6 j/hr-m^3-N/m^2 (5.9×10^6 Btu/hr-ft^3-atm)
Combustion equivalence ratio	LBO $< \phi_0 < 1.0$	> 1.0
Overall equivalence ratio	LBO $< \phi_0 < 1.0$	0.34
Air split for cooling	N. A.	30%
Air split for dilution	N. A.	38%
Premix reference velocity	157.8 m/s (518 ft/s)	N. A.
Premix Mach number	0.28	N. A. (0.27 at compressor discharge)
Premix dwell time	1.4 ms	N. A.
Premix length	22.3 cm (8.8 in.)	N. A.

[a]G.E. CF6-50. Data from Ref. 12.
[b]Takeoff conditions.
[c]At overall equivalence ratio = 0.34.

Fuel Injection/Premix Section. As is seen from Fig. 6, premixing is carried out via a coaxial flow scheme where the fuels are injected at the bell mouthed entry to a 5.25-cm (2.07-in.) diameter straight cylindrical duct, 10.16 cm (4.0 in.) long. The flow area provides a space velocity of about 140 m/s (460 ft/s) for the cruise power condition. This results in a residence time for premixing of about 1.6 ms from the injection plane to the flameholder exit plane.

The fuel injector is a JPL-fabricated device designed to inject liquid jet fuel and either gaseous H_2 or a simulated partial oxidation product gas into the air stream from injection tubes arranged to provide a near-uniform initial distribution of fuel over the cross section of the mixing duct. Figure 8 shows photos of the injector assembly with both the H_2/JP and gas/JP versions of the injector head. The H_2/JP head was used throughout the hydrogen-enrichment experiments reported here.

The H_2/JP injector head utilizes 15 pairs of coaxial tubes as shown in Fig. 8(c). The jet fuel is injected from the innermost tube of each pair and the hydrogen is injected from the annulus between the inner and outer tubes. The inner tube is 2.11-mm (0.083-in) O.D. with a 0.25-mm (0.010-in) wall thickness and the outer tube is 3.18-mm (0.125-in) O.D. with a 0.25-mm (0.010-in) wall thickness. The exit end of each pair of tubes is located approximately at the throat station of the bell-mouthed entry. This positioning of the injection tube ends, combined with an appropriate location of the conical surface of the injector head, provides an arrangement where the fuels are injected into a region of near-axial air flow. Turbulence and recirculating flows are thus deliberately avoided in the mixing duct in order to reduce flame holding tendencies under the high temperature and pressure of the inlet air.

Atomization of the liquid-fuel streams is accomplished by reversing the usual scheme for pressure atomizers where high-velocity fuel is injected into low-velocity air. In the present scheme, advantage is taken of the high-velocity air which is required for short premix residence times, and the fuel is injected at low velocities: of the order of 3 m/s (10 ft/s). Thus a large velocity gradient is available for fuel atomization, and a volume mean drop diameter of ~ 25 μm is predicted using the Nukiyama-Tanasawa correlation (Ref. 13). The coaxial arrangement of the injected flows and the near-axial air flow also reduces the sensitivity of the fuel distribution to variations in flow rates as operating conditions are varied.

The improvement in premixing performance of this coax injection scheme relative to the previously used pneumatic atomizer which was located at the entrance to the same air-inlet bellmouth (Ref. 4 and 5) was evaluated in ancillary cold flow tests with both injectors at fixed flow rates under ambient temperature and pressure conditions. Water was

---

[4]In order to reduce the effects of cooled walls on emissions and blowout limits, the cooling system was designed to maintain a relatively high (~ 810 K) (1000°F) gas-side wall temperature.

Figure 8(a). Separable coax injector for JP5 with neat H_2 or simulated gas fuels.

Figure 8(b). Separable coax injector for JP5 with neat H2 or simulated gas fuels (cont.).
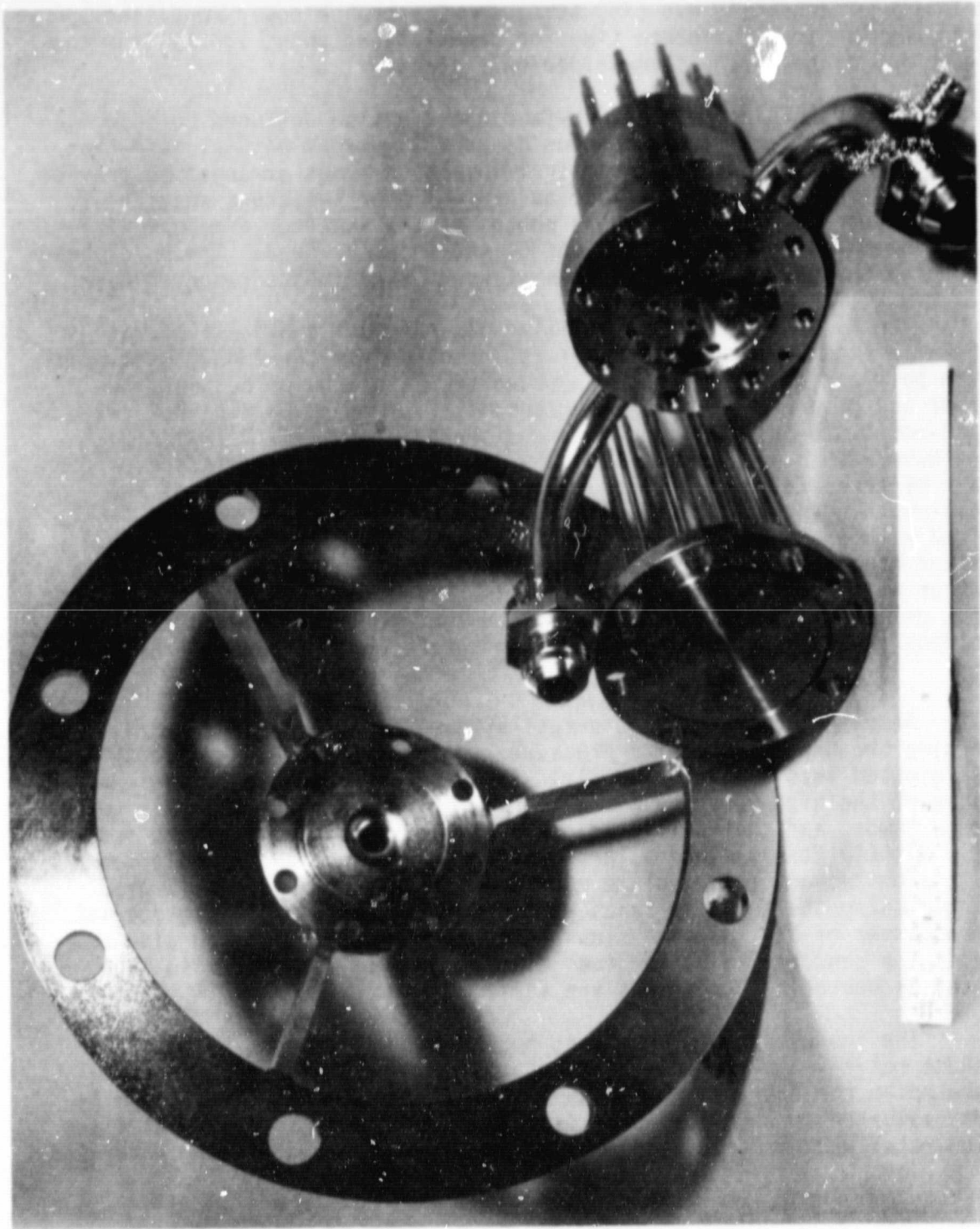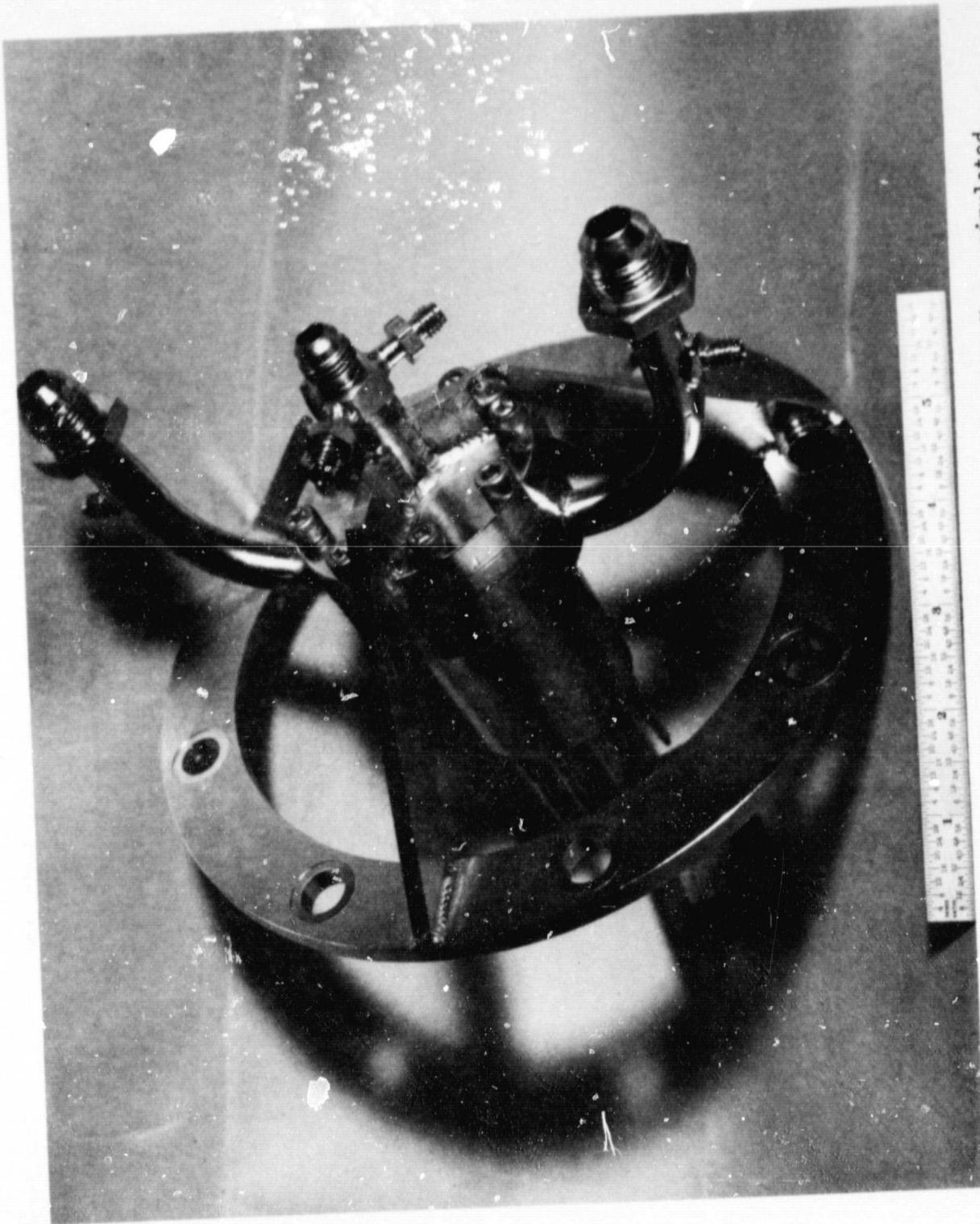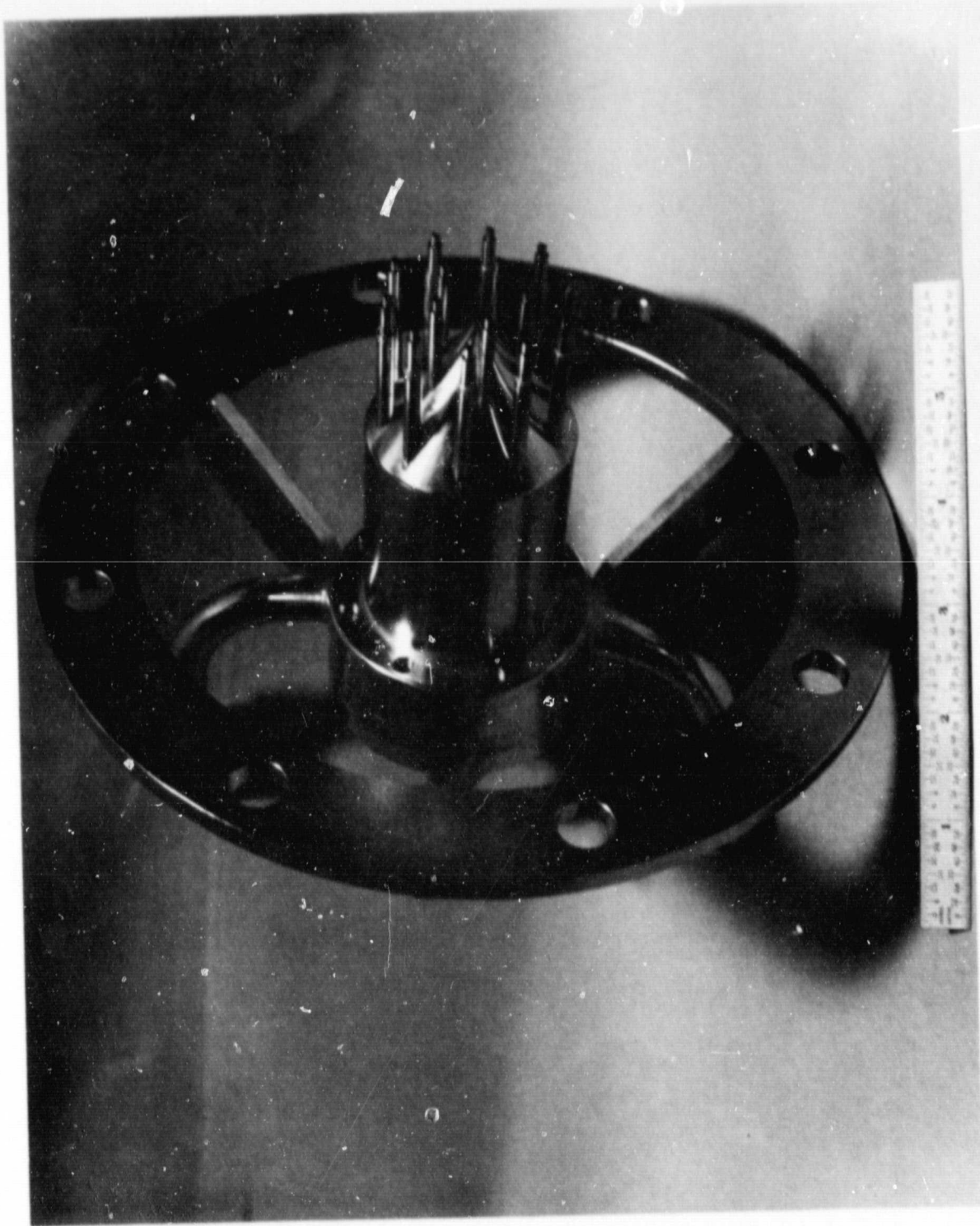
Figure 8(c). Separable coax injector for JP5 with neat H₂ or simulated gas fuels (cont.).
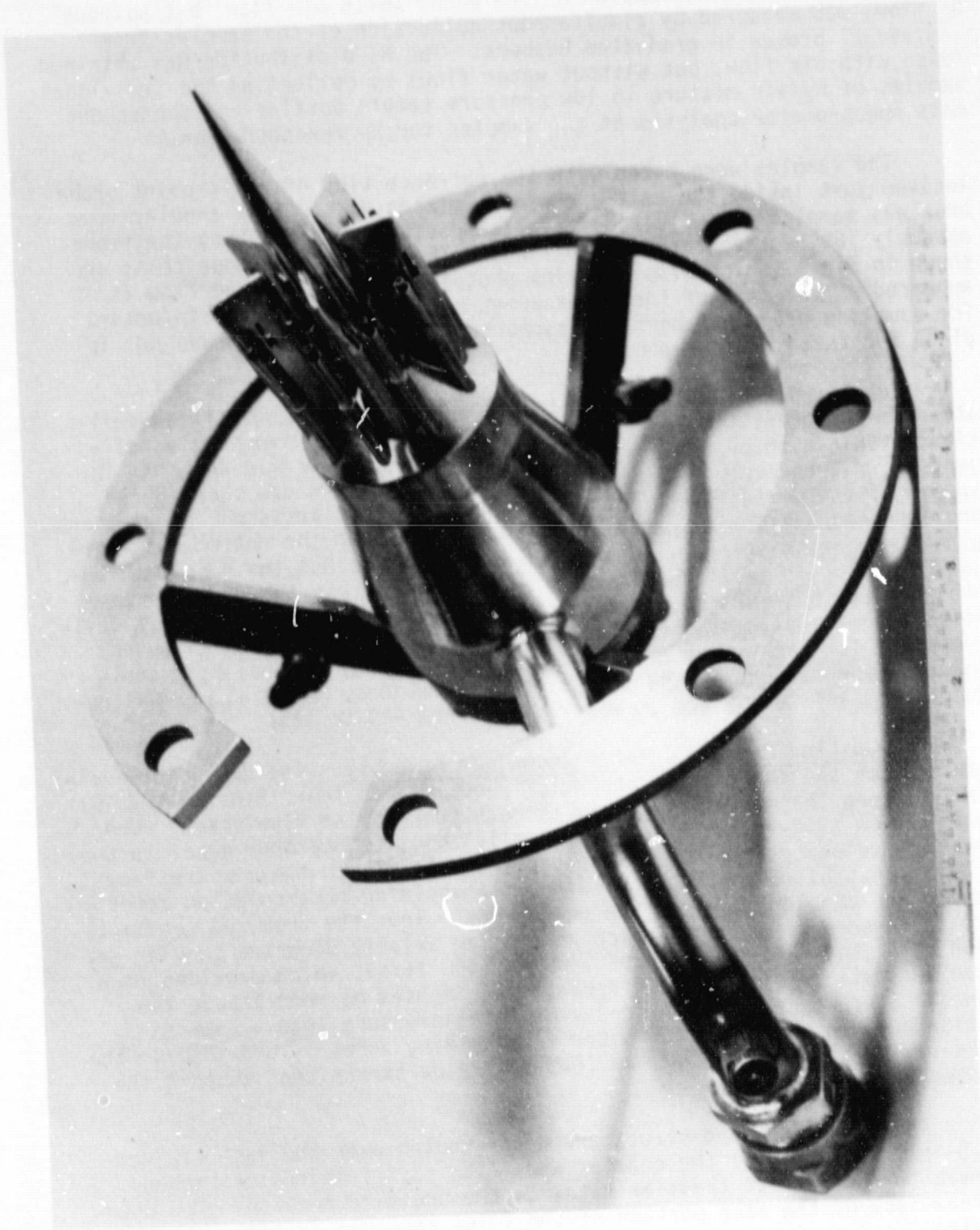
Figure 8(d). Separable coax injector for JP5 with neat H₂ or simulated gas fuels (cont.).

substituted for the jet fuel. The tests were conducted by sampling the flow at the median radius of six equal-area annuli across the flow area of a 20.3-cm (8.0-in.) long, 5.08-cm (2.0-in.) diameter transparent mixing duct. The distribution of the water (with air flow, but without H_2 flow) was measured by simultaneous collection of the samples from individual probes in graduated beakers. The H_2 distribution was obtained (also with air flow, but without water flow) by collecting the individual samples of H_2/air mixture in low pressure sample bottles and subsequent mass spectrometer analysis of the samples for H_2 concentration.

The samples were taken with the entrance tips of a six-point probe located just inside the exit end of the mixing duct. Each annular flow area was sampled at two circumferential positions by rotating the probe assembly 180 degrees between samplings. The results of these tests are shown in Fig. 9 which also contains photographs of the mixed flow as it appeared at the exit of the transparent mixing duct for each injector. The sampling probe was normally supported by the flange but was not in place for these photographs.

The bars in Figs. 9(a) and (c) show the range of normalized deviation of the quantities of sampled components for the two sample positions within each of the six equal areas for the pneumatic and coax injectors, respectively. The most striking differences are the reduced spread of the deviations of both components in each increment of area and the improved uniformity of the H_2 distribution over the entire duct area with the coax injector. The water distribution across the duct with the coax injector is still considerably less uniform than the H_2 but is improved over that for the pneumatic atomizer injector. The standard deviation (σ) of the sample sets (one set of 12 samples for each injected component for each injector) as shown on Figs. 9(a) and (c) is a semi-quantitative measure of the foregoing observations, where σ_{water} was reduced from 44% to 35% and σ_H was reduced from 41% to 12%.

Combustion Chamber Inlet/Flameholder Assembly. The design criteria adopted for the combination step/bluff-body flameholder (Figs. 6 and 10) were to keep the mixture velocity through the annular flow area around the 7.62-cm (3.0-in.) diameter, semi-ellipsoidal centerbody equal to the approach velocity from the mixing duct, and to direct the mixture flow so as to establish roughly equivalent flameholding recirculation zones behind the annular step and the centerbody. Thus the premixed reactants are introduced to the combustion zone as an axially directed annular jet with velocities of the order of 140 m/s (460 ft/s), which provides more than adequate resistance to flashback yet imposes no more than a reasonable (for concept evaluation) 7-8% total pressure loss. Communication between the inner and outer flameholding zones is provided in the wake region behind four 1.27-cm (0.5-in.) wide struts that support the centerbody.

The centerbody and struts are water-cooled over the last 1.27-cm (0.5-in.) of length at the chamber end. The cavity in the centerbody serves to reduce heat transfer rates to the uncooled portion. The downstream face of the step portion of the inlet assembly is also water-cooled.

Acoustic cavities of quarter-wave slot configuration are positioned around the periphery of the inlet section, adjacent to the chamber wall. Half of them are sized for the first tangential acoustic mode frequency of the chamber and the other half tuned for the second tangential mode. This cavity design was found to be adequate to control high-frequency (3-5 KHz) combustion resonance.

Combustion Gas Sample Probe and Sample Analysis. On-line analysis of combustion gas composition was accomplished by means of a water-cooled probe, an electrically heated sample transfer line, and various gas analysis instruments. Gas samples were analyzed on a dry volumetric basis using chemiluminescence, FID, and NDIR instruments for NO_x, HC, and CO and CO_2, respectively. A paramagnetic instrument was used for O_2 concentration analysis.

The water-cooled probe is mounted through the exhaust nozzle, as shown in Fig. 6, on the centerline axis of the combustor. The choked-entry orifice of the probe is located a fixed 30.48 cm (12.0 in.) from the face of the chamber inlet assembly and in the subsonic approach flow to the nozzle sonic plane. Cooling provided by the choked-entry flow and by the water-cooling passages in the probe reduced the temperature of the gas-sample stream to less than 478 K (400°F) one meter (3 ft) downstream of the probe entrance for all run conditions.

The total sample from the probe is transferred to the analysis instruments via a heavy-walled, stainless-steel tubing about 91 m (300 ft) long. The walls of the tubing are heated to 420 K (300°F) with a low-voltage ac electrical current. The line is vented to the atmosphere at the location of the analysis instruments after a small portion of the gas sample is withdrawn for analysis.

Experimental Procedure and Operating Conditions. The emissions data were obtained during runs of 1-to 3-hr duration with constant inlet-air conditions typical for a cruise-power setting, nominally 1.18 MPa (11.6 atm) and 728 K (850°F), except for a few experiments with air conditions typical of takeoff power, nominally 3.04 MPa (30 atm) and 811 K (1000°F). The range of operating conditions for the hydrogen-enrichment experiments is summarized in Table 4(a). Because of the constant area exhaust nozzle, it was necessary to modulate the air mass flow rate as the equivalence ratio was varied in order to maintain a nearly constant inlet air pressure in the plenum. For that purpose, airflow rates were varied from 1.46 to 1.78 kg/s (3.22 to 3.93 lbm/s) and from 3.79 to 4.03 kg/s (8.36 to 8.89 lbm/s) for cruise and takeoff conditions, respectively.

All experimental data were digitally recorded on magnetic tape and subsequently reduced by computer. Each data point was obtained with flow conditions held constant until gas analysis, which was continuously monitored, indicated steady values. See Appendix C for calculation procedures.
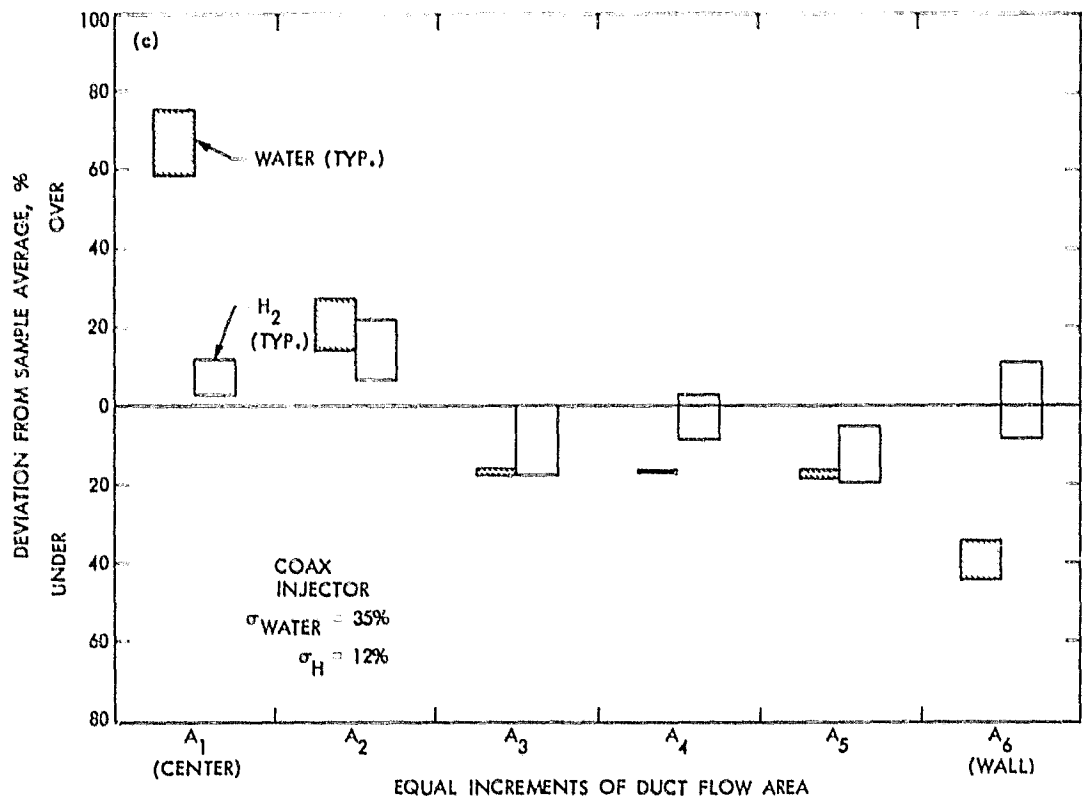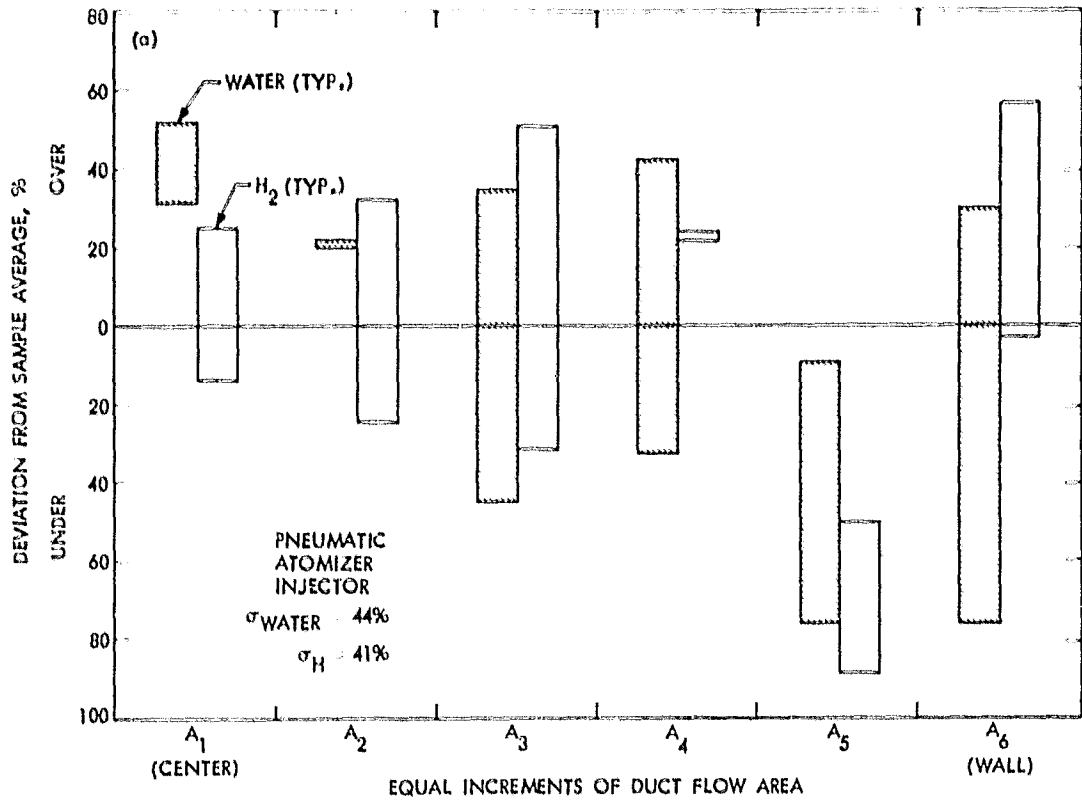
Figure 9. Cold-flow mixing test results for the coax and pneumatic atomizer injectors for H_2/JP fuels.

(b)

82-2

(d)

3
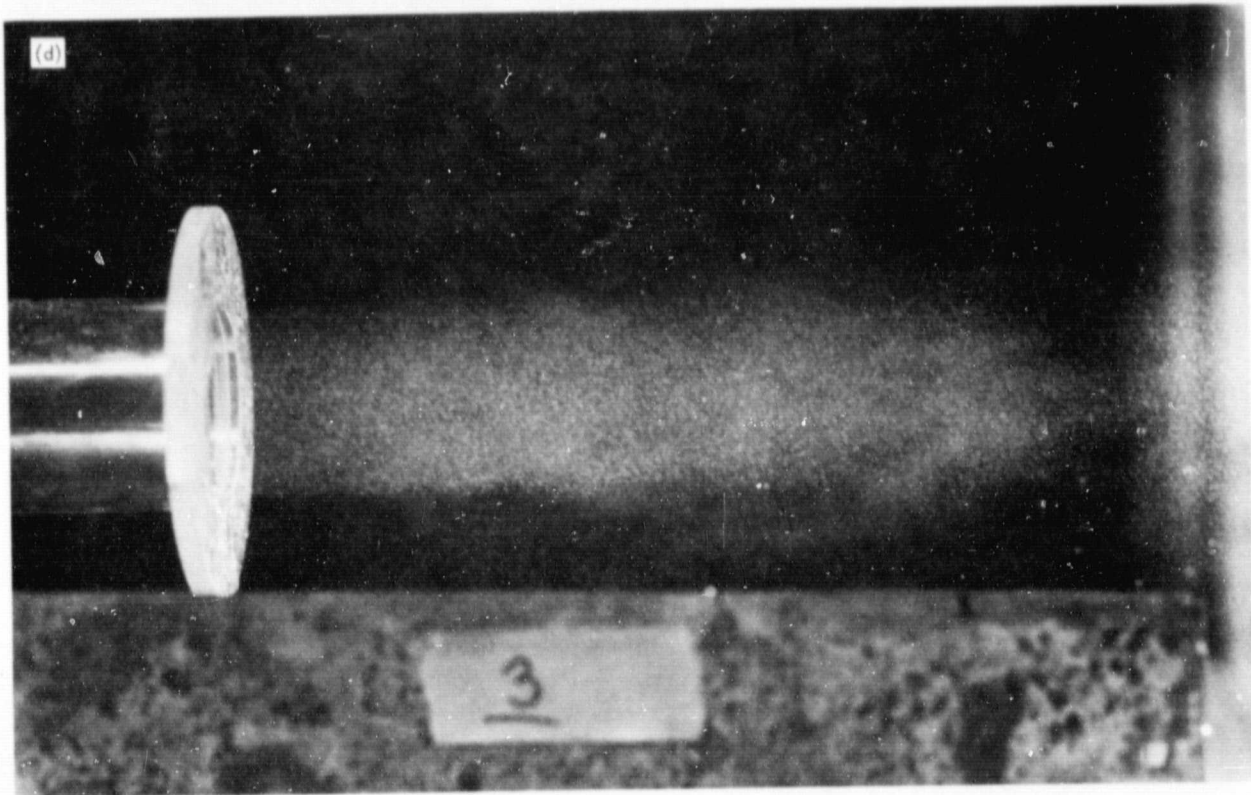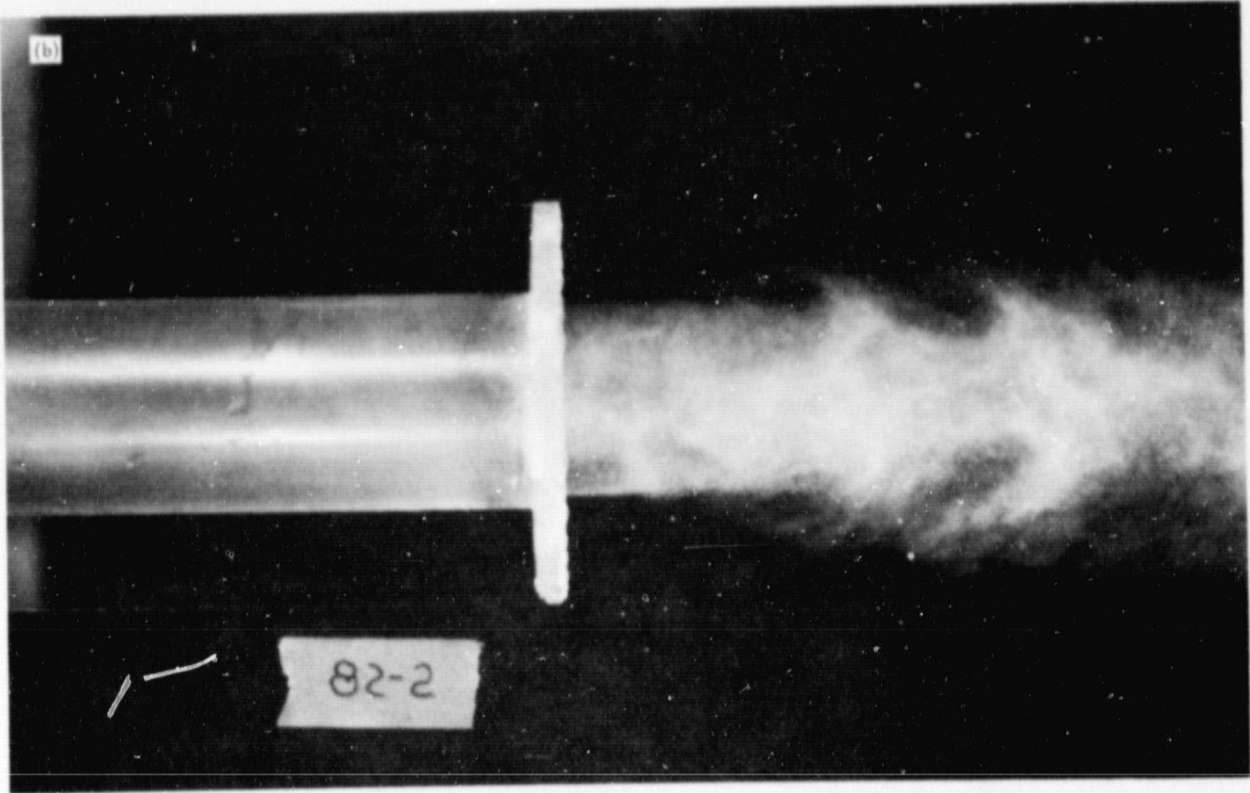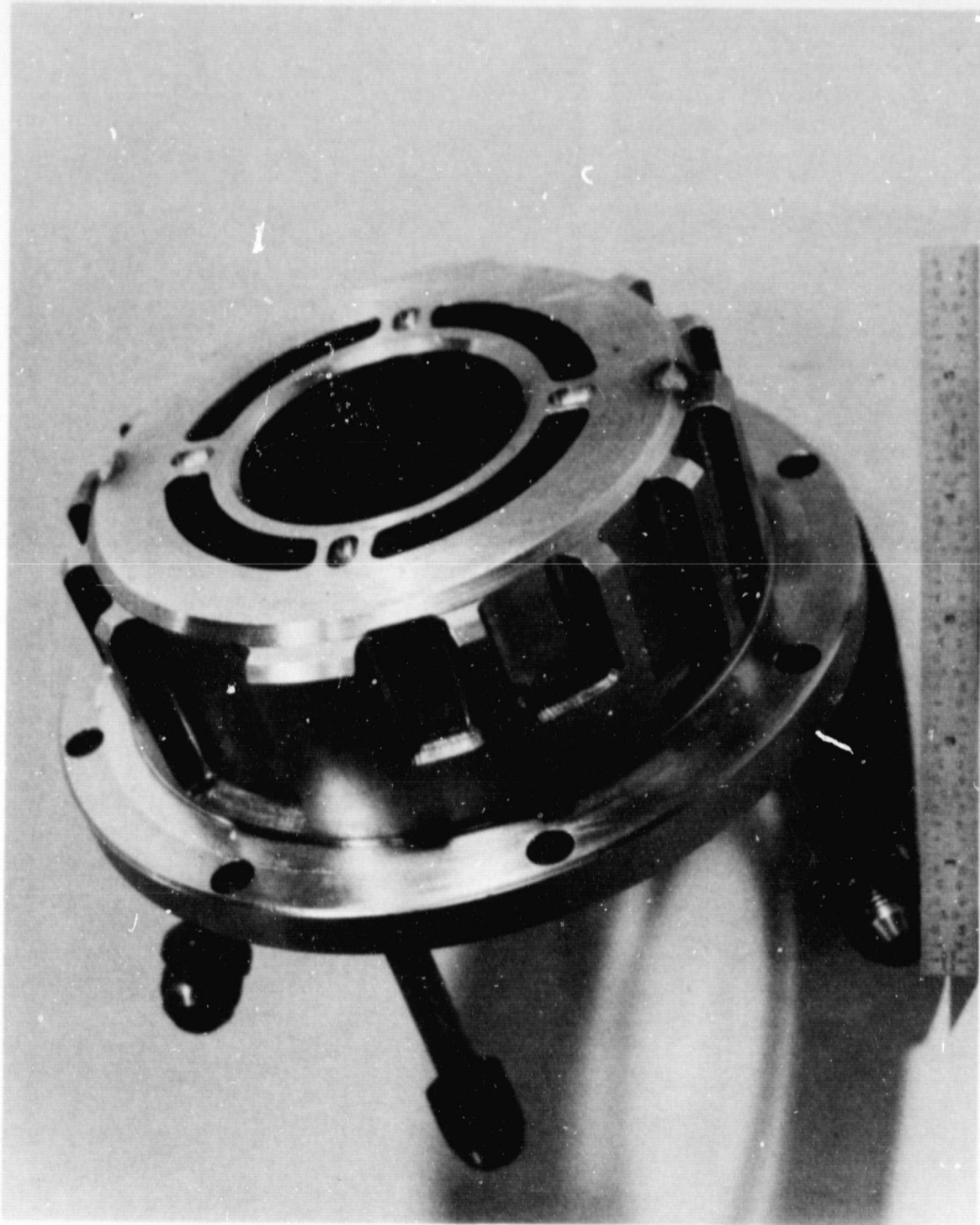
Figure 10. Water-cooled inlet/flameholder assembly.

Table 4. Summary of operating conditions.

| Fuel | Inlet Air | | Equiv. Ratio (ϕ_o) | Air Split (S_a)(a) | Fuel Split (S_f)(a) | H2 in Total Comb. | Premix Temp. (T_M) K (°F) | Total Press. Loss(b) |
	Press Mpa (atm)	Temp. (T_A) K (°F)						
(a) Hydrogen-enrichment experiments. H2/JP injector.								
JP5 only (Baseline)	3.00-3.13 (29.5-30.8)	811-816 (1000-1008)	0.45-0.61	Not applicable	Not applicable	0	759-777 (907-938)	6-8
H$_2$ + JP5	3.04 (29.9)	807 (993)	0.60	Not applicable	Not applicable	5	753 (896)	6
JP5 only (Baseline)	1.18-1.29 (11.6-12.7)	721-731 (837-856)	0.44(c)-0.72	Not applicable	Not applicable	0	683-694 (770-790)	6-7
H$_2$ + JP5	1.20-1.25 (11.8-12.3)	726-728 (846-851)	0.39(c)-0.61	Not applicable	Not applicable	4.7-5.7	683-694 (770-790)	6-7
(b) Simulated-gas experiments. Gas/JP injector.								
JP5 only (Baseline)	1.18-1.20 (11.6-11.8)	725-729 (845-852)	0.42(c)-0.72	0	0	0	683-694 (770-790)	6-9
Gas + JP5	1.15-1.21 (11.3-11.9)	723-727 (842-849)	0.48-0.61	5	24-30	2.2-2.6	672-678 (750-760)	7-8
Gas + JP5	1.21-1.26 (11.9-12.4)	825-827 (1025-1029)	0.39(c)-0.61	5	24-33	2.2-3.0	758-769 (905-925)	8-11
Gas + JP5	1.13-1.18 (11.1-11.6)	724-729 (844-852)	0.48-0.61	10	48-59	3.6-4.1	650-655 (710-720)	7-8
Gas + JP5	1.19-1.23 (11.7-12.1)	825-827 (1025-1028)	0.44-0.61	10	48-67	3.5-4.3	728-742 (850-875)	8-11
Gas + JP5	1.09-1.10 (10.8-10.9)	726-729 (847-852)	0.49(c)-0.58	15	71-77	5.0-5.3	631-639 (675-690)	7-8
Gas only	1.07-1.12 (10.6-11.0)	727-728 (848-851)	0.49(c)-0.60	18-21	100	5.6-5.7	603-631 (635-675)	7-9
Gas only	1.10-1.19 (10.9-11.7)	824 (1023)	0.49(c)-0.60	15-21	100	5.7-5.8	578-703 (761-805)	8-10

aAir and fuel to first stage are calculated values based on maintaining a constant first stage equivalence ratio = 2.83.
bAs % of inlet air total pressure.
cLean blowout.

2. Experimental Results

Emission results for the cruise-power operating condition are shown in Fig. 11 where it can be seen that:

a. The ultralow emission goals are simultaneously achieved or bettered over an equivalence ratio range (based on H_2 + jet fuel) of 0.45 to 0.52 using 4.7-5.7 mass % H_2 (H_2 in total fuel).

b. The lean blowout limit (LBO) is reduced from an equivalence ratio of 0.44 for JP only to 0.39 with 5.5% H_2.

These data also show that the target emissions are simultaneously achievable with JP5 alone in the 0.48 to 0.55 equivalence ratio range with the good premixing obtained with the coax H_2/JP injector. However, the high level of mixedness produces a high LBO ($\phi_{LBO} \sim 0.44$), and the HC and CO levels are very sensitive to equivalence ratio as LBO is approached. Addition of the relatively small amounts of H_2 used here broadens the margin between acceptable blowout stability and acceptable emission levels. This broadened margin would be highly significant in a full-scale premixed combustor where gross fuel and air maldistributions exist.

The 4.7-5.7% H_2 used to obtain these results represents better than a 50% reduction in required H_2 from previous results (Refs. 4 and 5), and is within the range theoretically available from a very fuel-rich precombustion stage.

The results for the takeoff-power condition shown in Fig. 12 were obtained in a single run of 40 minutes duration. No evidence of pre-ignition was observed while obtaining the data shown in Fig. 12. However, while setting the flows for a leaner H_2 + JP data point a sudden increase in the mixing duct wall temperature occurred followed by a burnout in the proximity of the duct-wall expansion for the centerbody. This was evidently caused by flow separation at the radius of curvature of that transition. This radius was therefore increased when the inlet section was rebuilt, but further attempts to operate at the takeoff condition were not made in the interest of conserving the combustor hardware.

From Fig. 12, the NO_x emissions are approximately double those for the cruise condition at fixed equivalence ratio; however, the higher temperature and pressure of the combustion process suppress the typical upswing in CO and HC toward leaner equivalence ratios beyond the range of data obtained here, so that the trend toward a higher level of the NO_x emissions at takeoff might be overcome by leaning out the primary zone further.

The level of CO emissions was approximately the same as for the cruise condition, but the HC level was markedly greater. The latter result is contrary to the usual trend of decreased unburned HC with increased combustion temperature, but, since the level is still an order
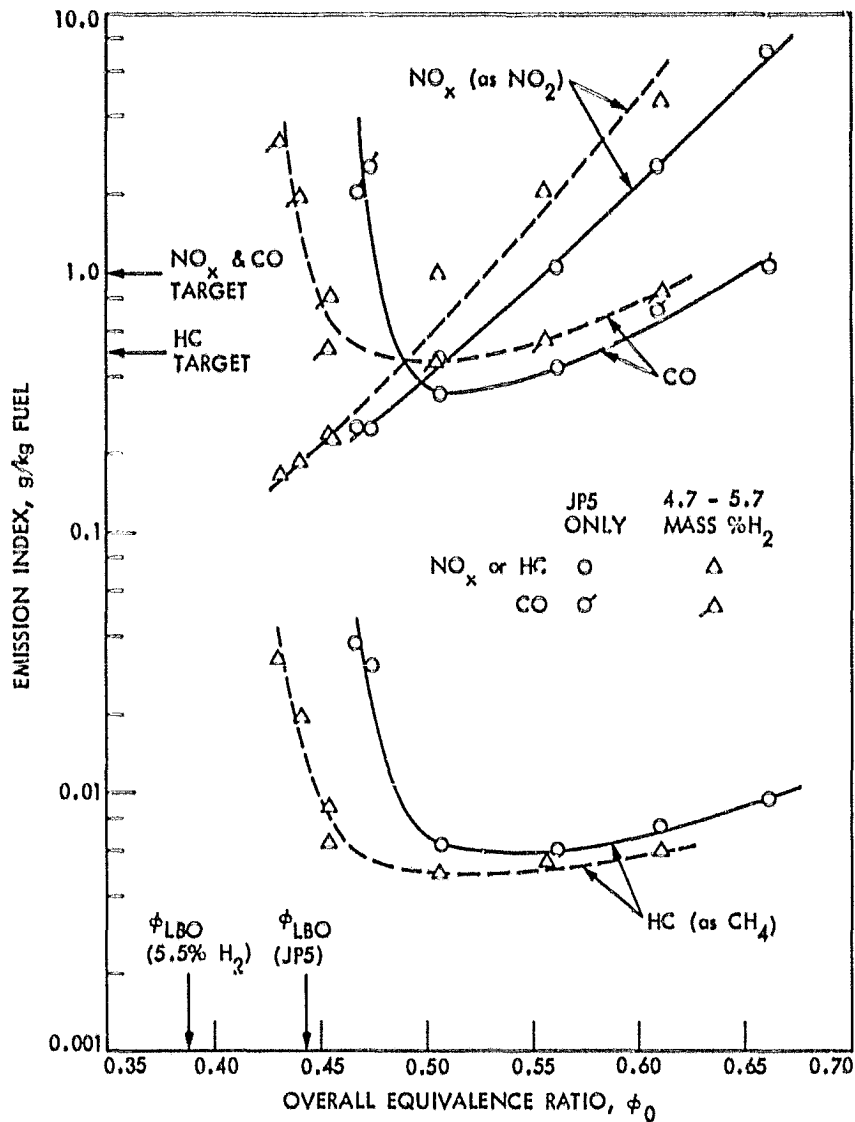
Figure 11. NO_x, CO, and HC emissions with and without hydrogen. Cruise power inlet-air conditions; 728 K ($850^\circ F$), 1.18 MPa (11.6 atm). H_2/JP injector.
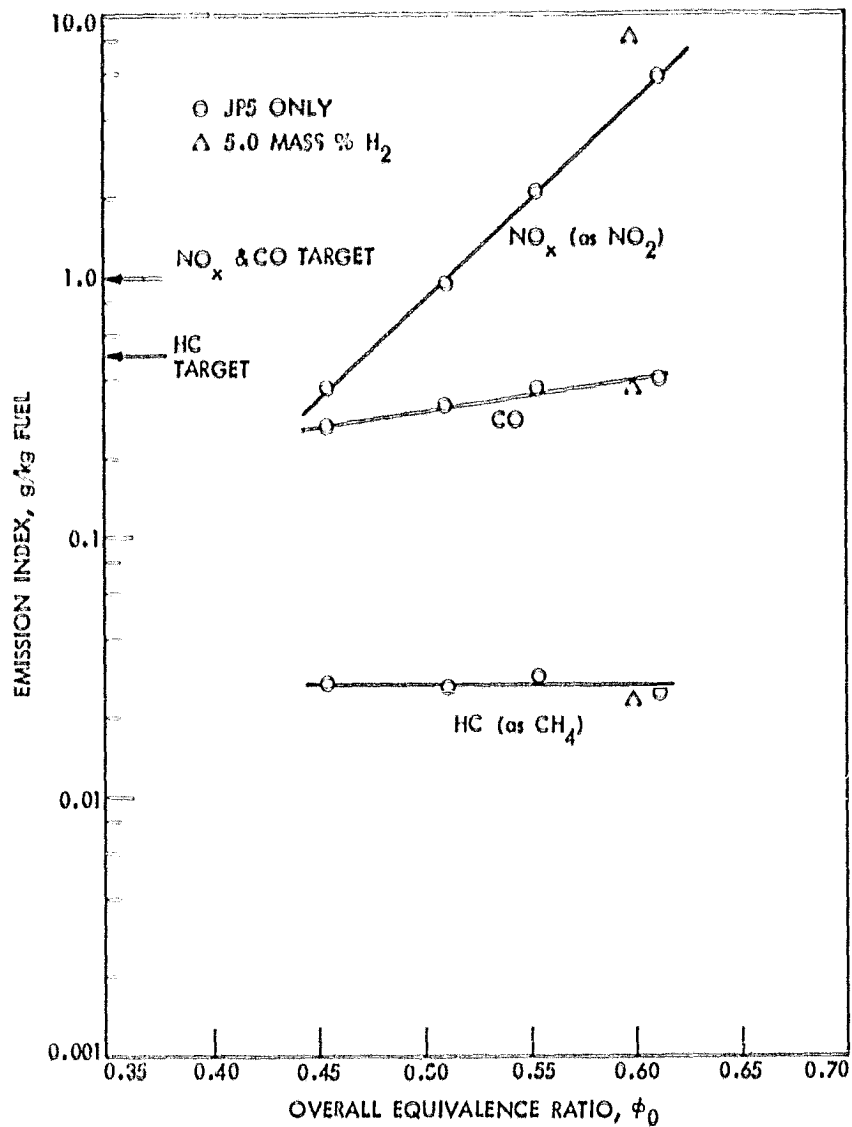
Figure 12. NO_x, CO and HC emissions with and without
hydrogen. Take-off power inlet-air conditions: 811 K
(1000°F), 3.04 MPa (30 atm). H_2/JP injector.

of magnitude below the HC emission target and is near the limit of measurement for the HC analyzer, a rational explanation for the result has not been pursued.

B.   SIMULATED-GAS EXPERIMENTS

1.   Description of Experiments

In order to verify that the lean-burning enhancement and ultralow emissions obtained from the foregoing experiments with neat-H2/JP could be retained upon substitution of a H2-bearing partial-oxidation product gas stream from a fuel-rich precombustion stage, a series of experiments were conducted using a simulated partial-oxidation product gas from a bottled source. It was expedient to use a simulated product gas in order to evaluate combustion properties because a very fuel-rich pre-combustion reactor suitable for operation under the inlet air conditions of interest in these experiments was not available.

The JPL MOD 2M combustor previously described (Figs. 6 and 7) was fitted with the gas/JP version of the fuel injector head (Fig. 8(d)) but otherwise was unchanged for these experiments.

Gas/JP Fuel Injector. The gas/JP injector head (Fig. 8d) is de-signed to inject either liquid jet fuel or fuel gas, or both simul-taneously, into the airstream with near-uniform initial distribution of flow over the cross section of the mixing duct. The design is func-tionally identical to that previously described for the H2/JP head, ex-cept for the addition of fuel gas injection tubes.

The fuel gas is injected into the airstream from 30 slots [7.5mm (0.297 in.) long x 1.6 mm (0.063 in.) wide] located near the closed ends of the five larger tube elements visible in Fig. 8(d), and from the 15 annular spaces surrounding the jet-fuel tubes. Flow from these latter spaces was retained not only to improve the initial distribution of gas flow but also to reduce the wakes behind the jet-fuel tubes when jet fuel was not used. The closed ends of the gas injector tubes were tapered to reduce wakes when gas was not flowing. A long, tapered ex-tension of the injector body was used to fill the space at the center of the injection array, further reducing circulation regions downstream of the injector.

Since the gas flow from the slots was transverse to the airflow, it was necessary to avoid high gas-to-air momentum ratios in order to suppress the formation of wakes by the gas flow and to reduce the sensi-tivity of the initial gas dispersion to variations in gas-flow rates. Consequently, the slots were sized to provide gas-to-air momentum ratios generally less than unity over the range of operating conditions.

Simulated Product Gas and Feed System. The nominal composition of the simulated product gas used throughout the experiments is shown in Table 1, where it is also shown to be essentially equivalent to the adiabatic equilibrium composition of the products from a reaction at an

equivalence ratio of 2.83. This stoichiometry is the theoretical optimum for production of H_2 without smoke, as was previously discussed. Since it was desired to maintain the theoretical H_2 content in the three-component product gas simulant, small adjustments to CO and N_2 content were made to account for the missing minor constituents of the actual product gas. These adjustments were made by combining all the inerts as N_2 and the CH_4 as CO.

The three gases were supplied to the combustor rig from individual high-pressure storage tube banks. A flow control system consisting of pressure regulators and critical flow metering nozzles maintained the desired flow proportions over the range of test conditions. The gases were combined and thoroughly premixed before entering the fuel injector.

No attempt was made to preheat the simulant gas prior to injection because a heater with adequate capacity was not available. Therefore, deficiency in thermal energy existed for the simulant, since the adiabatic temperature of the actual product gas is about 1422 K (2100°F). This condition was reflected as a reduced temperature in the combustor mixing duct and produced rather dramatic effects on combustor blowout limits and emissions. A partial compensation for the thermal deficiency and an estimate of the dependency of NO_x emission levels on premix temperature was obtained by overheating the inlet air for several runs.

Experimental Procedure and Operating Conditions. The emissions data were obtained in the same manner as was described for the hydrogen-enrichment experiments at the nominal cruise condition except for the runs with overheated air. In those cases the air temperature was increased to approximately 825 K (1025°F), the maximum available from the air supply system. Air flow rates were varied from 1.17 to 1.67 kg/s (2.57 to 3.67 lbm/s) in order to maintain nearly constant inlet air pressure in the plenum.

The range of operating conditions for the experiments is summarized in Table 4(b), which expresses overall equivalence ratio (ϕ_0) and air and fuel split ratios as if the simulant gas were produced by a precombustion stage operating at a constant 2.83 equivalence ratio. As seen from Table 4(b), three modes of combustor operation were investigated: (a) JP5 only, a baseline operating condition; (b) fuel-gas only, a limit mode where processing all fuel through a precombustion stage was simulated; and (c) three levels of constant air split, where intermediate levels of fuel processing (i.e., precombustion stage throughput) were simulated.

The experimental premix temperatures (TM) shown in Table 4(b) can be compared to the predicted TM for actual two-stage operation shown in Table 5. Note that for the gas-only condition, increasing the air temperature (TA) to 825 K (1025°F) still left a deficit of 189-282 K (340-507°F) from the actual two-stage prediction for TM. For the smallest air split condition (5%), however, the overheated air boosted TM to within ~ 30 K (59°F) of the predicted TM.

Table 5. Estimated premix temperatures (TM) for various two-stage operating modes; cruise condition.

| Overall Equiv. Ratio (ϕ_0) | TM, K (°F) | | | |
| | Constant Air Split (%) | | | All Fuel to First Stage |
	5	10	15	
0.3	791 (964)	849 (1068)	a	854 (1078)
0.4			a	892 (1146)
0.5			902 (1164)	927 (1208)
0.6				960 (1268)

aInvalid operating condition.

Assumptions:

1. No reaction in premixing section and complete adiabatic mixing.

2. Inlet air: 1.2 MPa (12 atm), 728 K (850°F).

3. Constant first stage equivalence ratio = 2.83.

4. Thermochemical equilibrium product gas composition (Table 1) and temperature (1422 K (2100°F)).

5. Constant specific heats for air and product gas:

   Cp air = 336 J/kg K (0.26 Btu/lbm°F)
   Cp gas = 529 J/kg K (0.41 Btu/lbm°F)

6. Temperature effects of liquid fuel evaporation (constant air splits) are negligible.

2.   Experimental Results

Although the design of the liquid jet-fuel portion of the gas/JP injector head was nearly identical to that of the H_2/JP head, the presence of the five fuel-gas injection tubes and of the centerline fairing could alter the mixing of the jet fuel with the air (hence, the emissions) relative to that for the H_2/JP head. Therefore, new baseline emissions data for JP5 only were obtained using the gas/JP injector head. These data are shown in Fig. 13 where they are compared to the baseline curves for the H_2/JP injector previously discussed (Fig. 12). A trend for somewhat higher levels of all emissions is clear for the gas/JP injector. The increased NO_x together with the reduced ϕ_{LRO} suggest somewhat poorer premixing.

The NO_x, CO, and HC emission results for the fuel-gas experiments are summarized as a function of overall equivalence ratio in Figs. 14, 15 and 16, respectively, where they can be compared to the baseline emissions (dashed curve) for the combustor when fueled with JP5 only. The baseline data are omitted to reduce congestion of the figure. Data for standard 728 K (850°F) inlet air are shown with unflagged symbols and data for the overheated (825 K or 1025°F) inlet air are shown with flagged symbols. Emission index and overall equivalence ratio for the fuel-gas data are presented as if the combustor were operating as a two-stage system (see Appendix C for calculation procedure). Therefore, the fuel-gas data can be directly compared with the JP5-only data, except for the premix temperature effects. The equivalency of this comparison from a reaction chemistry viewpoint was consistently verified throughout the experiments by standard chemical balance techniques using the measured input flow rates and the measured composition of the exhaust gas. Agreement well within +10% was generally observed.

When the combustor was operated with the fuel gas under the standard air temperature condition of 728 K (1025°F), NO_x emissions (Fig. 14) were dramatically lowered from the baseline operation with JP5 only, mainly because of the reduction of mixture temperature and hence combustion temperature. In order to establish a normalization factor for this temperature effect, the NO_x results from fuel-gas-only runs with overheated air (825 K or 1025°F) were used to quantitatively estimate the temperature dependency. The form of the normalization factor was suggested by results reported in Ref. 14 and by the essentially parallel trend lines for NO_x under the hot and cold mixture condition as evidenced by the two lower trend lines in Fig. 14. The temperature dependency derived was $EINO_x \sim 10^x$ where x is TM/257 with TM in kelvins. Thus to estimate NO_x levels that would be obtained in a true two-stage system with predicted TM as shown in Table 5, the following expression was used:

$$(EINO_x)_{normalized} = (EINO_x)_{measured} \times 10^{(TM_H - TM_C)/257}$$

where TM_H = predicted TM and TM_C = experimental TM.
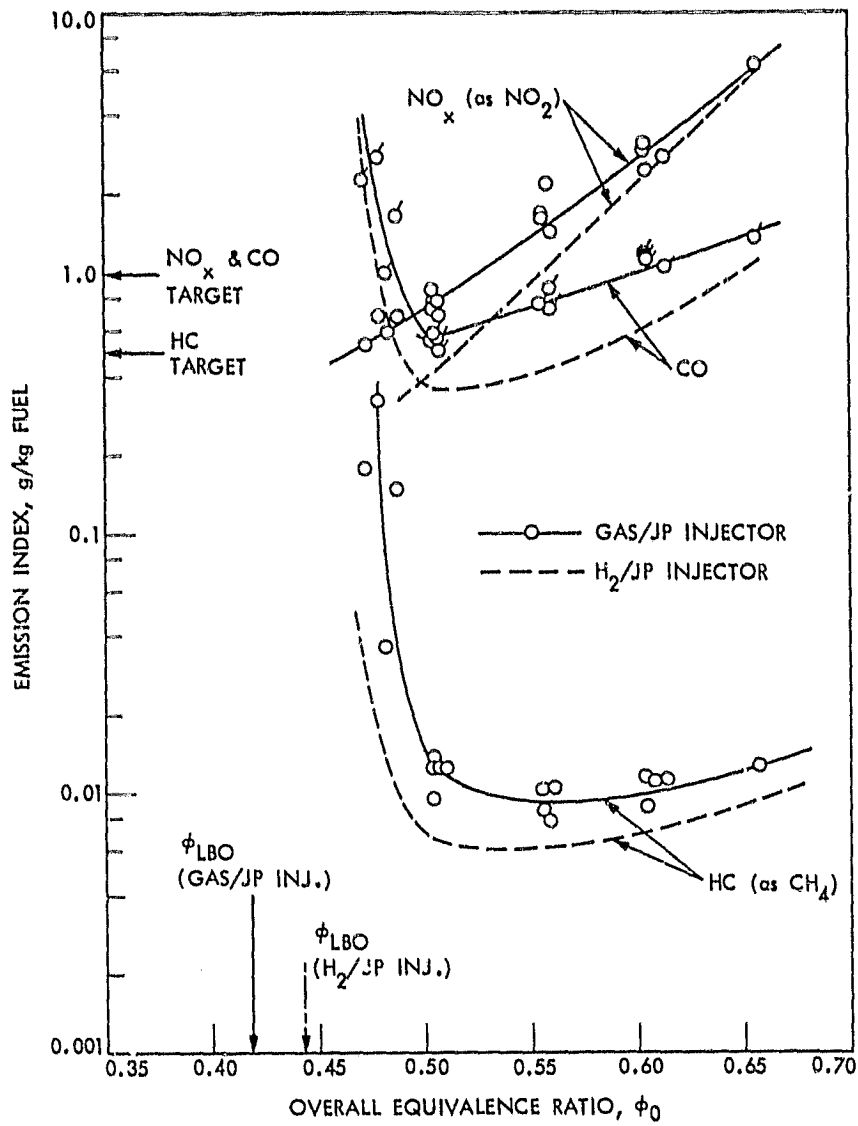
Figure 13. NO_x, CO and HC emissions with JP5 only. Cruise power inlet-air conditions: 728 K (850°F), 1.18 MPa (11.6 atm). Gas/JP injector.
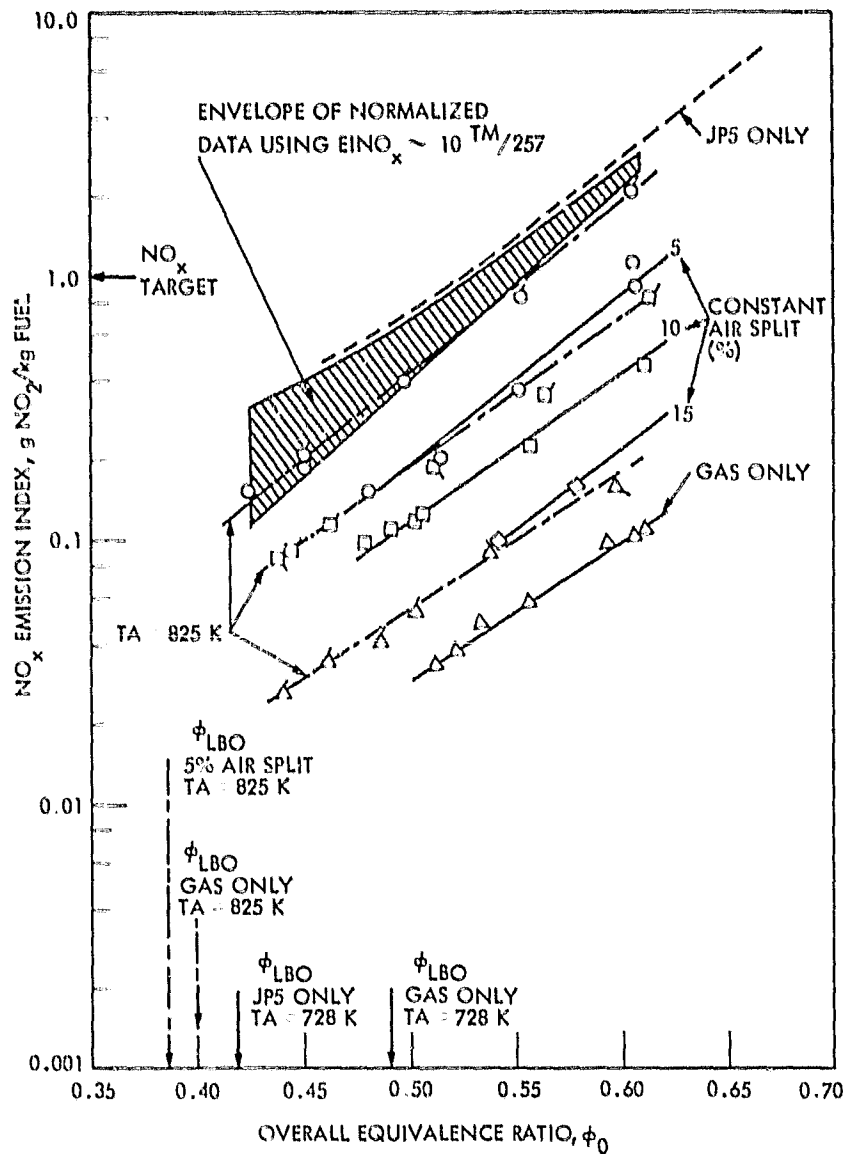
Figure 14. NO$_x$ emissions for various simulated pre-combustion-stage throughput levels. Inlet air conditions: 1.18 MPa (11.6 atm), 728 K (850°F) or 825 K (1025°F) as noted. Gas/JP injector.
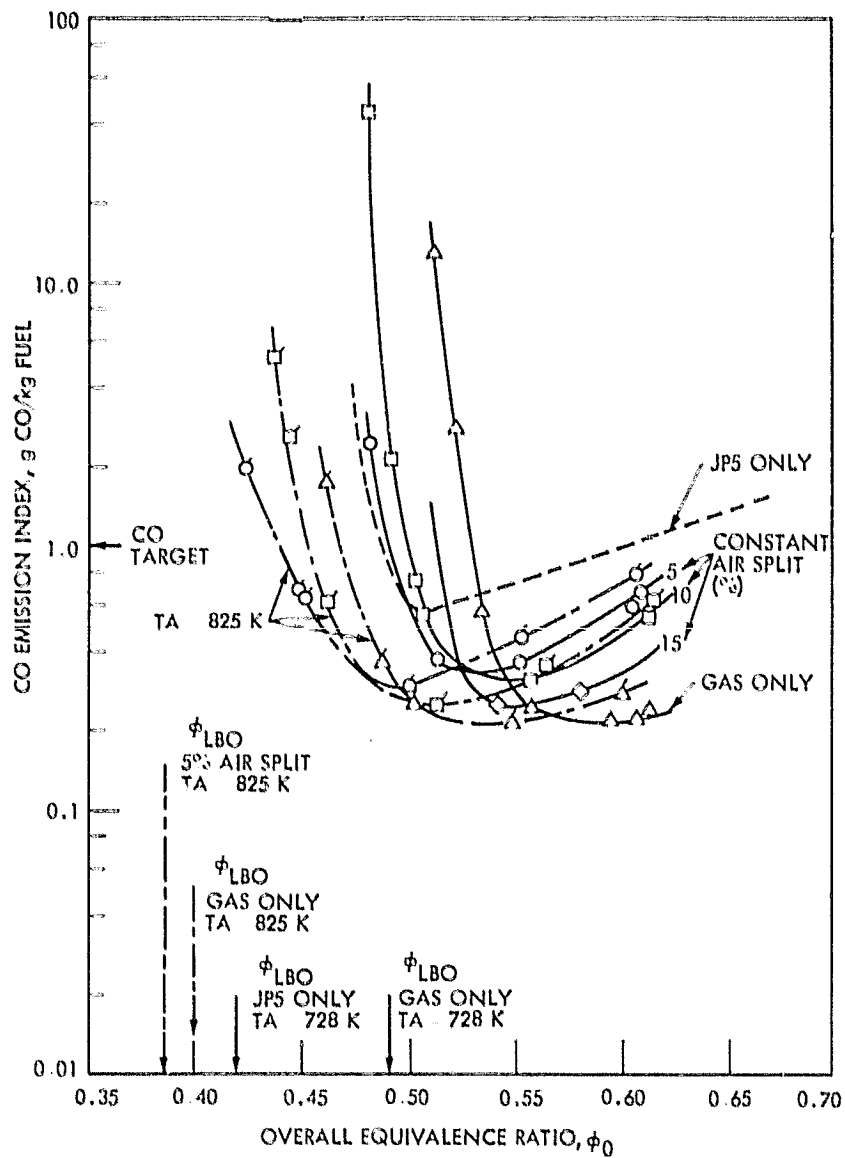
Figure 15. CO emissions for various simulated pre-
combustion-stage throughput levels. Inlet-air
conditions: 1.18 MPa (11.6 atm), 728 K (850°F)
or 825 K (1025°F) as noted. Gas/JP injector.

3-25
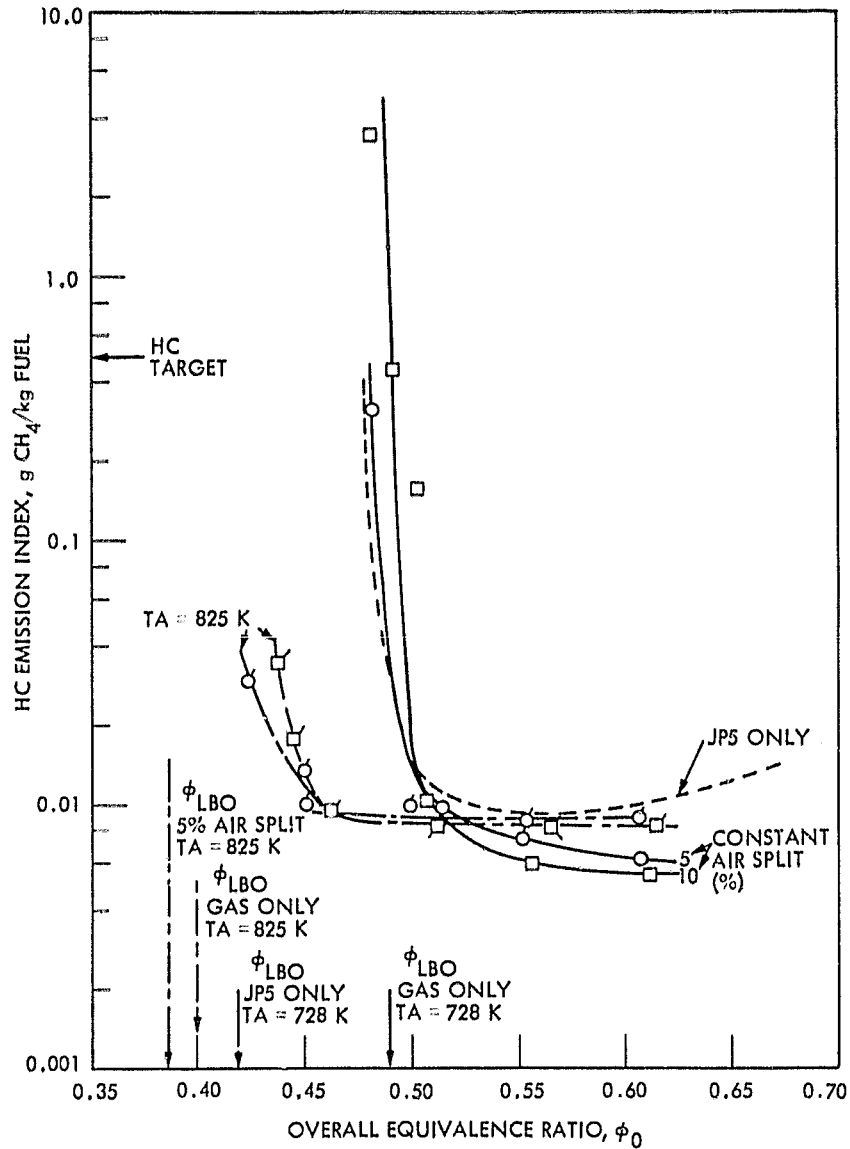
Figure 16. HC emissions for various simulated pre-combustion-stage throughput levels. Inlet-air conditions: 1.18 MPa (11.6 atm), 728 K (850°F) or 825 K (1025°F) as noted. Gas/JP injector.

The result of applying the above equation to the measured NO_x data for all of the fuel-gas runs is shown by the crosshatched envelope in Fig. 14. Although the necessity for the extrapolation may lessen the accuracy of these results, two considerations are believed to lend credence to the position of the envelope below the JP5 baseline curve. The first is the enhanced premixing effectiveness associated with the use of the gaseous fuel and the second is the complete absence of nitrogen intermediates in the fuel-gas because it was not produced chemically.

Perusal of the lower equivalence ratio portions of Figs. 15 and 16 shows that the CO and HC emission trends as well as LBO were also dramatically affected by the premix temperature when fuel gas was used. With the standard TA of 728 K (850°F), the onset of rapid increase of CO and HC emissions (indicating approach of LBO) and ϕ_{LBO} were improved markedly relative to the JP5-baseline data. These improved lean burning combustion characteristics are a central argument for the two-stage concept.

A quantitative correlation of these results with TM in the operating region where CO and HC emissions are changing rapidly has not been derived. However, the trend of the results suggests that further improvements in ultralean burning characteristics would occur for the higher levels of fuel-gas throughputs if TM were equivalent to the predicted two-stage values.

At the higher equivalence ratios, a small but consistent increase in CO and HC emission levels was observed for the fuel-gas runs when the inlet air temperature was increased (Figs. 15 and 16). A rational explanation for this apparently contradictory trend has yet to be found.

Interestingly enough, the ϕ_{LBO} of 0.386 for the 5% air-split case with $TM_C \simeq TM_H$ (overheated TA), where total combustibles were 2.2% H_2, nearly duplicates the previously established $_{LBO}$ for neat H_2/JP5 with 5.5% H_2. This suggests that substantial overall combustion enhancement could be realized without processing all the fuel through the precombustion stage of a two-stage system. This mode of operation is an important design option because, in principle, it eliminates the need for variable air split and requires only a variable fuel split to maintain a constant first stage equivalence ratio, a potential reduction in complication of two-stage combustor design. The result also suggests that a somewhat leaner burning precombustion stage could be employed which would alleviate sooting and flame stability problems with ultrarich combustion.

In summary, the results of the simulated product gas experiments suggest that, relative to premixed single-stage (JP-only) combustion, use of a very fuel-rich precombustion stage to precondition a large portion of the fuel, combined with effective premixing before final combustion, would significantly improve the margin of combustion while maintaining ultralow emission levels. The results also show that the basic benefits of H_2 enrichment in extending lean burning limits and providing for ultralow emissions are retained and probably improved by implementation via two-stage combustion.

C. RICH-BURN STUDIES

The rationale of staged combustion for minimizing NO_x emissions as discussed above relies heavily on implementing well-controlled partial oxidation of the fuel. However, very fuel-rich combustion is still poorly understood and the dearth of experimental information leaves substantial gaps in the data on fuel-rich combustion. Consequently, a series of laboratory-scale experiments designed to characterize the critical equivalence ratio (ϕ_c), which is the highest ϕ for which the fuel/air mixture can be burned soot-free, and the amount of hydrogen produced as a function of ϕ, was conducted. N-heptane (Ref. 15), n-octane, n-nonane and iso-octane were investigated using a laminar flow burner, while JP5 was investigated using a turbulent burner.

1. Laminar Burner Experiments

Metered flows of vaporized liquid fuel and air, which were thoroughly premixed, were burned in a laminar-flow flat-flame burner (Fig. 17). The products of combustion, which contained hydrogen, passed up a glass chimney and exited to the atmosphere. The chimney prevented any secondary air entrainment and made possible a precise determination of ϕ. The product gas composition was analyzed by an on-line gas chromatograph. In a typical data sequence, H_2 concentrations would be measured as a function of ϕ until sooting was visually observed. The highest value of ϕ which burned soot free was recorded as ϕ_c. A more detailed description of the experimental system has been presented in Ref. 15.

Figures 18, 19 and 20 show data on hydrogen production as a function of the equivalence ratio for n-heptane, n-octane, and n-nonane, respectively. (Hydrogen yield for iso-octane fuel was not obtained in these experiments.) Also shown on the figures are the equilibrium hydrogen concentrations at the adiabatic flame temperature and the experimentally observed ϕ_c.

Actual hydrogen yields were ~10 vol% and showed only a weak dependence on ϕ. Computed equilibrium hydrogen concentrations were always greater than the measured values. For example, the predicted equilibrium H_2 concentration for n-octane is 15.0 vol% at $\phi = 1.98$ compared to the observed 10 vol%. The difference between the measured and predicted hydrogen concentrations is attributed to heat losses to the burner surface, which lowers flame temperature and subsequently lowers H_2 concentrations. As seen in Fig. 18, there is a drop in H_2 yield for $\phi > 2.0$ with n-heptane fuel. This was due to the presence of a metal plate inserted in the post flame zone to alter the flow field and prevent the formation of flamelets associated with incipient sooting (Ref. 15 and 16). It seems reasonable to assume that the lower H_2 yield at $\phi > 2.0$ is due to the additional heat losses to the plate and the further reduction of the temperature of the product gases in the post flame zone. N-heptane was the only fuel where the metal plate was used to extend ϕ_c (Ref. 15).

For all these fuels, the predicted equilibrium H_2 concentration decreases as the fuel molecular-weight increases so that, in one sense,
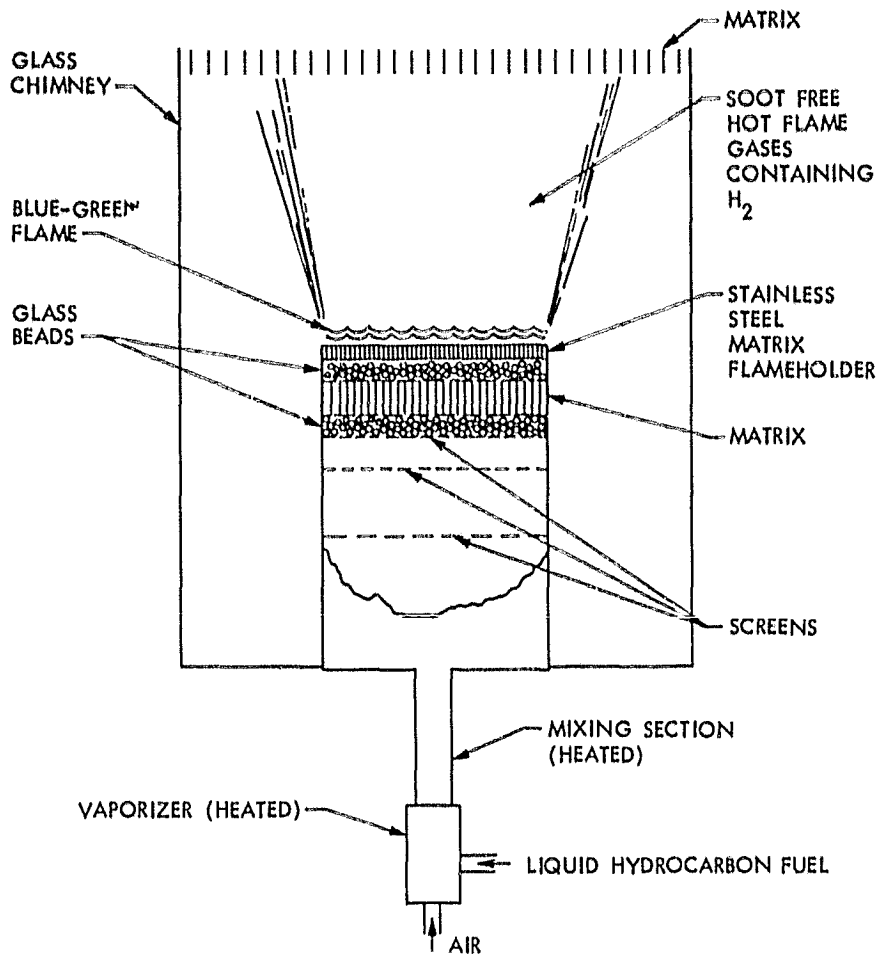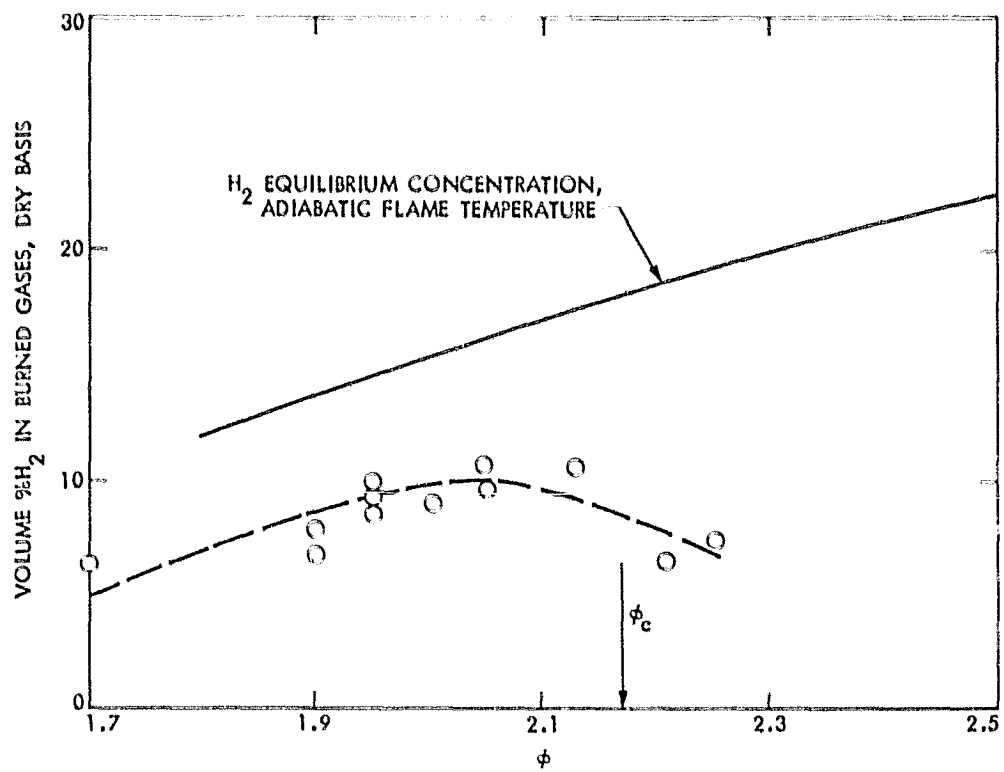
Figure 17. Schematic of flat-flame burner.

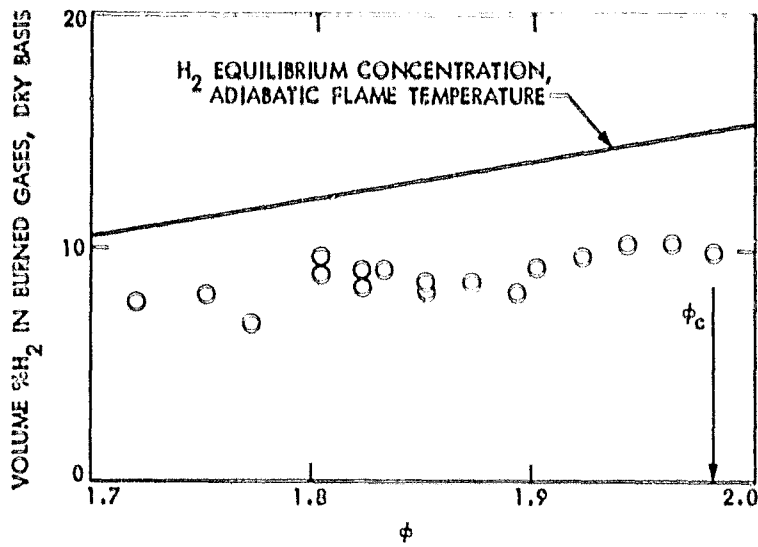Figure 18.   Hydrogen production vs. equivalence ratio, n-heptane fuel (Ref. 15).

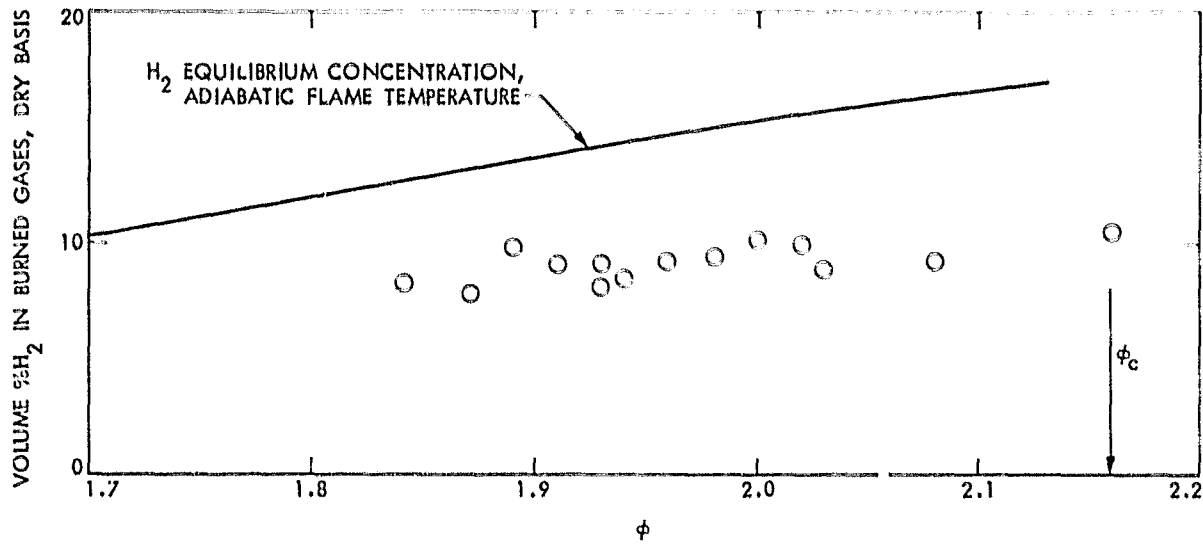Figure 19. Hydrogen production vs. equivalence
ratio, n-octane fuel.

Figure 20. Hydrogen production vs. equivalence ratio, n-nonane fuel.

the efficiency (defined as the observed H_2 concentration/equilibrium H_2 concentration) of this H_2 generation scheme appears to increase as the fuel molecular-weight approaches the jet fuel range. It is emphasized that thorough premixing of the fuel/air mixture is essential to achieve these results.

A chart tabulating critical equivalence ratios for the paraffin-series fuels tested is shown in Table 6. It is interesting to note there is only about a 10% variation in ϕ_c for these fuels, but this trend has not yet been verified for other fuel families (i.e. alkyl-benzenes). The values of ϕ_c presented in Table 6 for n- and iso-octane are higher than those reported by Street and Thomas (Ref. 17), who reported values of ϕ_c = 1.40 and 1.45 for n- and iso-octane, respectively. However, Street and Thomas refer to burning "mists" of hydrocarbon fuels and air in their experiments. If, in fact, the fuel was present as small droplets rather than a thoroughly premixed fuel/air mixture then the burning would not be premixed but diffusive in nature which would account for the lower value of ϕ_c. For further comparison, Blazowski, et al. (Ref. 18) has reported a value of ϕ_c = 1.70 for premixed iso-octane/air mixtures burned in a jet stirred reactor.

2.   Turbulent Burner Experiments

Although the flat-flame burner is attractive for laminar-flame studies, its utility as a prototype precombustion stage is limited. This is due to the inherently low mass throughput associated with this type of burner. The only way to increase the mass throughput while maintaining laminar flow is to increase the burner size. This is an unattractive feature for staged-combustor applications. Consequently, a turbulent-flow burner was constructed for the investigation of the rich-burning behavior of JP5 fuel.

A schematic of the turbulent burner is shown in Fig. 21. As in the laminar burner, liquid-hydrocarbon fuel (JP5) and air were thoroughly premixed and the fuel vaporized in a heated mixing section. Typical Reynolds numbers of the mixture in the mixing section were in the range of 6000-10,000. The mixture was then ignited and the combustion products, which contained hydrogen, passed up the chimney. As before, the outside chimney reduced secondary air entrainment. The inner chimney further excluded secondary air and provided some flame stabilization. The product gases were sampled by a water cooled probe and analyzed by a gas chromatograph to determine H_2 concentration. Two distinct classes of flameholders were used in these experiments: wake producing devices (bluff bodies and V-gutters) and swirlers. Qualitatively, both classes worked equally well; furthermore, among the wake producing devices, there was no apparent difference in rich-flame stability (at $\phi \sim 2.0$) between V-gutter and bluff body stabilized flames. This is in general agreement with the observations of Ozawa (Ref. 19), who presented data showing that the flame stabilization capability of a variety of wake producing shapes (V-gutters, cones, disks, etc.) was only a weak function of flameholder geometry for equivalence ratios from 0.4 to 1.6. For all of the data presented below, a vane type swirl flameholder ($S \sim 0.7$) (Ref. 20) was used.

Table 6. Critical equivalence ratios for hydrocarbon fuels, laminar burner.

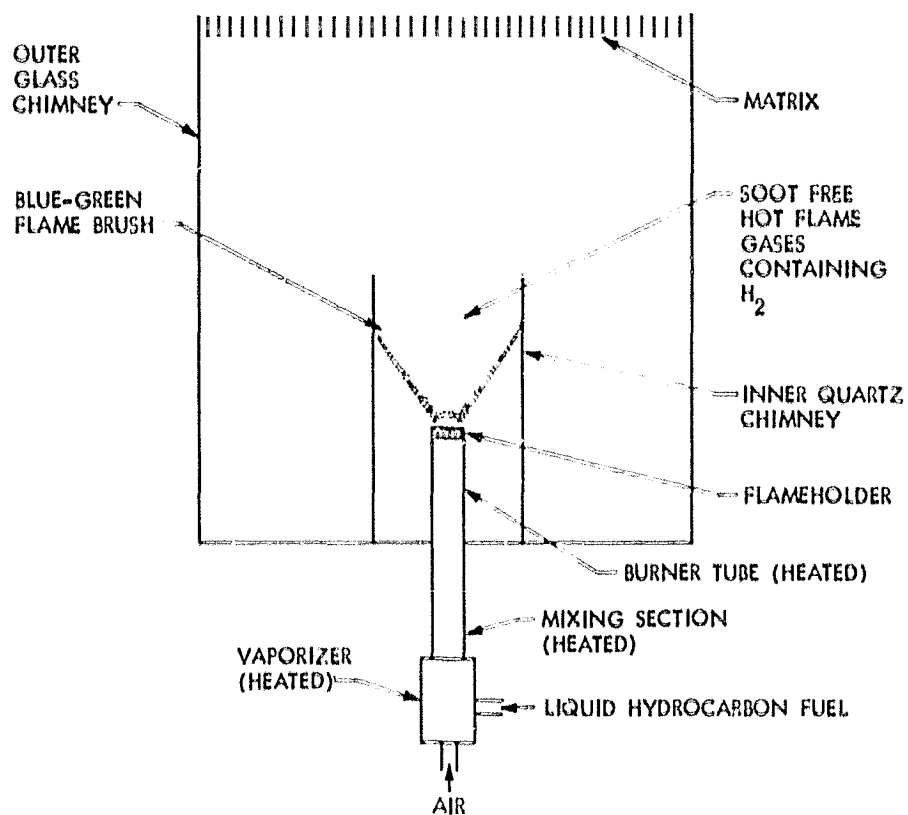| Fuel	Formula	ϕ_c
n-heptane	C_7H_{16}	2.17
n-octane	C_8H_{18}	1.98
iso-octane	C_8H_{18}	1.94
n-nonane	C_9H_{20}	2.16

Figure 21.   Schematic of turbulent burner.

Using the turbulent burner, the sooting equivalence ratio of JP5 was established at $\phi_c = 1.96-1.99$, the variation probably due to the fact that JP5 is a mixture of various hydrocarbon fuels. Experimental data on H_2 production for JP5 fuel is shown in Fig. 22. In this experiment the equivalence ratio was fixed at $\phi = 1.92$ and the hydrogen production as a function of fuel/air mixture temperature was measured. As seen in Fig. 22, the H_2 concentration increases as the temperature increases up to a value of 811 K (1000°F). Beyond this point, there is no measurable H_2 increase. This same trend was observed for a variety of inner chimney dimensions, and equivalence ratios. As seen in Fig. 22, H_2 yields varied from 6.5 to 7.2 vol% while equilibrium yields (not shown) varied from 11.67 vol% at 644 K (699°F) to 11.4 vol% at 811 K (1000°F). Visual observation of the swirl stabilized flame indicated that the flame stability increased as the inlet mixture-temperature increased. From a design standpoint, it is clear that the fuel/air mixture should be preheated as much as possible before ignition to maximize hydrogen production and flame stability.

The variation of H_2 production as a function of residence time, τ, is shown in Fig. 23. A small increase in H_2 yield is observed as τ increases from 2.3×10^{-2} s to 6.4×10^{-2} s. In these experiments, the inlet mixture temperature was 811 K (1000°F) and the equivalence ratio varied slightly from $\phi = 1.96$ to 1.99. It is assumed that the effects of the small changes in equivalence ratio are negligible. The residence time was calculated from $\tau = \ell/u$ where ℓ is the distance from the swirler exit plane to the probe and $u = \dot{m}/\rho A$ is the mass averaged axial velocity, with $\dot{m}$ the total inlet mass flow rate (fuel and air), ρ the mean product gas density calculated from adiabatic equilibrium conditions, and A the flow area of the inner chimney. Typically, $\ell \sim 7-20$ cm (2.76-7.87 in.), $\dot{m} \sim 1.75$ gr/sec. (3.86×10^{-3} lbm/s), $A \sim 28.3$ cm^2 (4.39 in.^{2}), and $\rho \sim 1.53 \times 10^{-4}$ gr/cm^3 (9.55×10^{-3} lbm/ft^3) at p = 0.101 MPa (1.0 atm), and T = 1950 K (3050°F). It is recognized that the residence time presented here is not a unique choice since the time spent in the recirculation zone is neglected. However, since this data is gathered at nominally fixed values of ϕ and $\dot{m}$, the time spent in the recirculation zone is approximately constant so that including recirculation would change τ only by a constant and the trend of H_2 yield against τ would be the same. From the data, it appears that the production of soot-free molecular hydrogen is favored as the residence time in the post-flame zone is increased.

3.   Conclusions From Rich-Burn Studies

Based on the data presented, the following conclusions are drawn:

a.   The sooting equivalence ratios for the paraffins n-heptane, n-octane, iso-octane and n-nonane have been measured on a flat flame burner. The measured values are comparable to or greater than those observed by previous investigators (Ref. 17 and 18).

b.   Hydrogen yields for these paraffins (except for iso-octane) have been measured and are typically 10 vol%, showing little
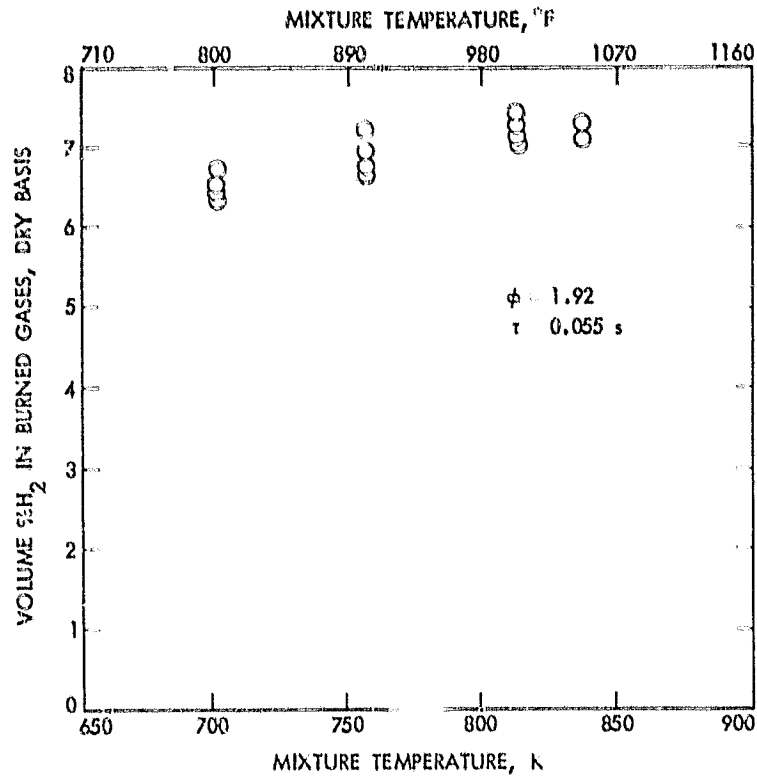
Figure 22. Hydrogen production vs. inlet mixture temperature, JP5 fuel.
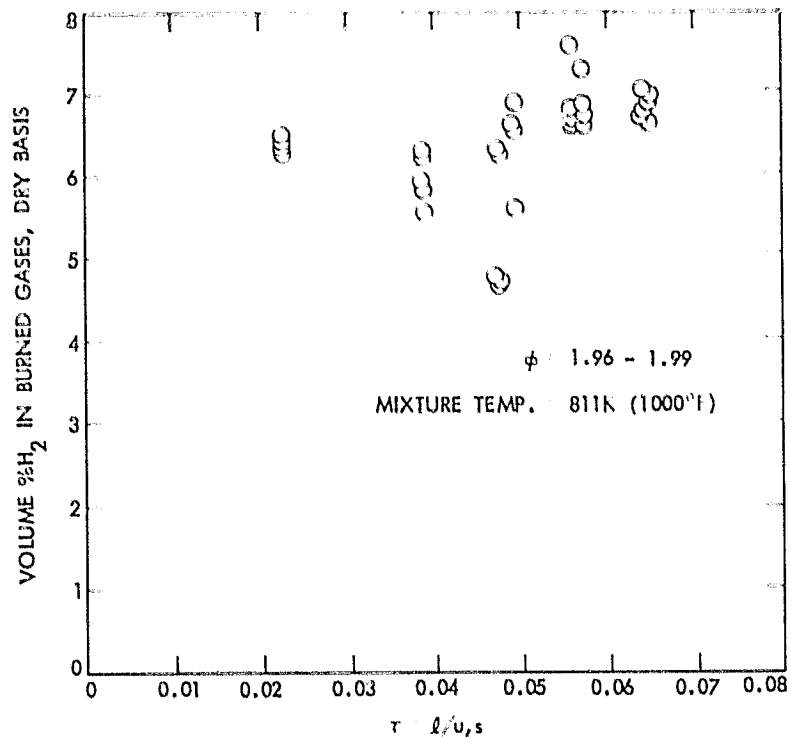
Figure 23. Hydrogen production vs. residence time, JP5 fuel.

dependence on equivalence ratio. This is lower than the value predicted by equilibrium thermodynamics for the individual fuels tested. The discrepancy is attributed to heat losses to the burner surface which lowered flame temperatures and lowered H_2 yields.

c.   The sooting equivalence ratio for JP5 is 1.96-1.99 measured on turbulent burner. This value is only weakly dependent on flame-stabilizer geometry.

d.   Hydrogen yields measured on the turbulent burner for JP5 fuel were typically 6-7 vol%. There is a slight but measurable increase of H_2 yield as the inlet fuel/air mixture temperature or residence time in the post flame zone is increased.

SECTION IV

CONCLUDING REMARKS

A partial oxidation staging concept for broadening the combustion margin between ultralow emissions and the lean stability limit for gas turbine combustion has been described and elements of its experimental verification have been accomplished. While the practical feasibility of the concept was not verified because a complete two-stage combustor was not operated, the following conclusions can be stated from results to date.

1. Ultralow levels of NO_x, CO, and HC emissions can be achieved in a premix combustor using JP5 only, but for simultaneously minimized levels of all three species very little combustion margin remains. This lack of margin would be very significant in an engine combustor where large mixture ratio variations are present due to nonuniform airflow distribution from the compressor.

2. Admixtures of neat H_2 with conventional JP5 jet fuel provide a significant extension of the lean blowout limit. The proportion of H_2 in the total combustibles required to achieve ultralow levels of emissions simultaneously with the extended lean limits is within the theoretical capabilities of a very fuel-rich partial oxidation process.

3. Use of a very fuel-rich precombustion stage to precondition a large portion of the fuel, combined with effective premixing of all reactants before final combustion, would permit the retention, and probably the enhancement of the basic benefits of H_2 enrichment.

4. Soot production is likely to be a major obstacle to operation of a precombustion stage beyond an equivalence ratio of 2.0. However, the results from the experiments with the simulated product gas from a reaction at $\phi = 2.83$ suggest that somewhat leaner precombustion could be employed to provide substantial enhancement of the final combustion.

REFERENCES

1. Aircraft Engine Emissions, NASA Conference Publication 2021, National Aeronautics and Space Administration, 1977.

2. Fundamentals of Gas Turbine Combustion, NASA Conference Publication 2087, National Aeronautics and Space Administration, 1979.

3. Premixed Prevaporized Combustor Technology Forum, NASA Conference Publication 2078, National Aeronautics and Space Administration, 1979.

4. Clayton, R. M., Reduction of Gaseous Pollutant Emissions From Gas Turbine Combustors Using Hydrogen-Enriched Jet Fuel - A Progress Report, Technical Memorandum 33-790, Jet Propulsion Laboratory, Pasadena, CA, October 15, 1976.

5. Clayton, R. M., "Hydrogen Enrichment for Low-Emission Jet Combustion," Evaporation and Combustion of Fuels; Advances in Chemistry Series 166, pp. 267-286, American Chemical Society, Washington, D. C., 1978.

6. Clayton, R. M., Performance Evaluation of a Catalytic Partial Oxidation Hydrogen Generator Using Turbine Engine Fuels, Technical Report AFAPL-TR-77-62, Air Force Aero Propulsion Laboratory, Air Force Systems Command, United States Air Force, Wright-Patterson AFB, OH, October 1977.

7. Clayton, R. M., "A Partial Oxidation Staging Concept for Gas Turbines Using Broadened Specification Fuels," Paper 79-GT-169, Presented at the ASME 24th Annual International Gas Turbine Conference, San Diego, CA, March 12-15, 1979. Also appears in J. of Engineering for Power, Vol. 102, No. 2, pp. 427-433, April 1980.

8. Clayton, R. M., "Emission Characteristics of a Premix Combustor Fueled with a Simulated Partial-Oxidation Product Gas," Paper 79-1322, Presented at the AIAA/SAE/ASME 15th Joint Propulsion Conference, Las Vegas, NV, June 18-20, 1979.

9. Yamagishi, K., et al., "A Study of NO_x Emission Characteristics in Two Stage Combustion," 15th Annual Symposium (International) on Combustion, The Combustion Institute, pp. 1157-1166, 1975.

10. Gordon, S., and McBride, B. J., Computer Program for Calculation of Complex Chemical Equilibrium Compositions, Rocket Performance, Incident and Reflected Shocks, and Chapman-Jouguet Detonations, NASA SP-273, Lewis Research Center, Cleveland, Ohio, 1971.

11. Coward, H. F., and Jones, G. W., Limits of Flammability of Gases and Vapors, Bulletin 503, Bureau of Mines, Washington, D. C., 1952.

12. Rudey, R. A., Status of Technological Advancement for Reducing Aircraft Gas Turbine Engine Pollutant Emissions, NASA TMX-71846, Lewis Research Center, Cleveland, OH, December 1975.

13. Nukiyama, S., and Tanasawa, Y., "Experiments of the Atomization of Liquids in an Air Stream," Defense Research Board, Dep:. of National Defense, Ottawa, Canada, March 19, 1950. [Translated from Transactions of the Society of Mechanical Engineers (Japan), Vols. 4, 5, and 6, 1938-1940, by E. Hope.]

14. Roffe, G., Effect of Inlet Temperature and Pressure on Emissions From a Premixing Gas Turbine Primary Zone Combustor, NASA CR-2740, September 1976.

15. Ryason, P. R., "Extended Soot Limits for Rich n-Heptane/Air Flames," Combustion and Flame, Vol. 29, 329-331, 1977.

16. Markstein, G., "Instability Phenomena in Combustion Waves," Fourth Symposium (International) On Combustion, The Combustion Institute, pp. 44-60, 1953.

17. Street, J. C., and Thomas, A., Fuel, Vol 34, 4-36, 1955.

18. Blazowski, W. S., Edelman, R. B., and Harsha, P. T., Fundamental Characterization of Alternate Fuel Effects in Continuous Combustion Systems: Technical progress report for period August 15, 1977 - August 14, 1978, prepared for U. S. Department of Energy Contract EC-77-C-03-1543, Exxon Research and Engineering Co., Linden, N. J., September 1978.

19. Ozawa, R. I., Survey of Basic Data on Flame Stabilization and Propagation for High Speed Combustion Systems, the Marquardt Co. Tech. Report AFRPL-TR-70-81, Van Nuys, CA, pp. 1-68, January 1971.

20. Beer, J. M., and Chigier, N. A., Combustion Aerodynamics, Halsted Press, Division of John Wiley & Sons, Inc., New York, pp. 122-130, 1972.

APPENDIX A

FUEL NO_x CONSIDERATIONS

A. INTRODUCTION

In the future, it is likely that alternative liquid fuels derived from coal or shale syncrudes will supplement existing petroleum-based fuel stocks for gas turbines. Minimally processed fuels refined from syncrudes will differ from their petroleum derived counterparts in physical properties and in chemical makeup. Generally speaking, the alternative fuels will be less volatile and will contain less hydrogen and a greater amount of fuel-bound nitrogen. These differences can have significant impact on gas turbine combustor performance from an environmental standpoint.

Lower volatility and reduced hydrogen content will tend to increase the emissions of HC, CO and smoke from the turbine combustor, but those fuel characteristics probably can be accommodated by conventional combustor development approaches. Fuel-bound nitrogen, on the other hand, is not easily accommodated since combustion chemistry less amenable to control is involved in the conversion of fuel nitrogen to NO_x. Moreover, the production of so-called fuel NO_x tends to be additive to the thermal NO_x that is already a problem in gas turbine combustion.

Recently published data (Ref. A-1) shows that coal derived fuels emit up to twice as much NO_x as conventional No. 2 distillate oil when burned in a scale model of a stationary gas turbine. The same data also shows that the amount of NO_x increases with increasing nitrogen content in the liquid fuel. Similarly, increased levels of NO_x have been reported in experiments where shale-derived jet fuels were burned in full size gas turbine combustors (Refs. A-2 and A-3). These studies emphasize the continuing need for the development of new combustor design technology for the reduction of NO_x to environmentally acceptable levels.

The following sections will expand the idea of two-stage combustion to include its application for reducing both fuel and thermal NO_x. Section B will review the two-stage strategy and summarize what previous work may be of use in this particular application. Sections C and D will focus on the chemical processes in the first and second combustion stages, which are the heart of NO_x reduction.

B. TWO-STAGE RICH/LEAN COMBUSTION

As discussed in the main text of this report, staged combustion would employ two stages of reaction. In the first stage, premixed fuel and air would be partially burned under fuel-rich conditions, with the equivalence ratio being as high as possible without producing soot. The soot-free requirement limits the first-stage equivalence ratio to a maximum of ~2.8, depending on the fuel; i.e., for $\phi > 2.8$ equilibrium considerations predict soot in the combustion products. If equilibrium is attained at $\phi \sim 2.8$, the products of this partial oxidation stage

would be (by volume) H_2 ($\sim 23\%$), CO($\sim 25\%$), and noncombustibles such as CO_2($\sim 0.5\%$), H_2O($\sim 0.9\%$) and N_2($\sim 51\%$). This hot product mixture would then be mixed with additional air and burned to completion in the second stage under fuel-lean conditions.

Processing the fuel through a fuel-rich combustion stage has specific advantages from the standpoint of emission control. First, the H_2-content and the hot, fully gaseous state of the product gas extend the lean limit and increase the mixing and combustion rates for final combustion. These benefits enhance the stability margin available for reduction of thermal NO_x while retaining low HC and CO emissions as is discussed in the main body of this report.

Second, premixed, fuel-rich reactions suppress the formation of nitrogen-bearing intermediate compounds involved in the generation of fuel NO_x. From a combustion performance standpoint, their role is not large since their concentrations (generally less than 1%) are small. From an environmental standpoint, the importance of these compounds is immense. The breakdown of the fuel and fuel bound nitrogen into chemically active species that react to form intermediates that ultimately become final products (including pollutants) is further discussed in Section C.

Successful implementation of two-stage combustion could effectively decouple the properties of raw turbine fuel from the final combustion process, giving the combustor greater fuel flexibility. In the future, when a wide variety of fuels may have to be burned in the same combustor, this is a further distinct advantage.

The individual concepts used in the formulation of the two stage combustion strategy such as hydrogen production by rich, thermal partial-oxidation, soot-free rich burning, combustion of premixed air/H_2/CO mixtures at $\phi < 0.6$, and hydrogen enrichment for lean-blowout limit extension have been at least partially demonstrated in the work discussed in this report. Also, a two-stage combustor similar in concept to the one described above, but burning methane fuel, has been previously built (Ref. A-4). In this combustor, however, the fuel and air were not completely premixed, and thorough premixing of fuel and air should extend the sooting equivalence ratio (see Section III C of this report) and lower the concentration of certain pollutant-related chemical species (Ref. A-4).

C.   FIRST-STAGE RICH COMBUSTION

Many investigators have studied various aspects of pollutant species formation during rich burning. Studies covering premixed (Ref. A-4 - 14) and diffusive systems (Ref. A-4, 8, 12, 15 - 17), laminar (Ref. A-5 - 11, 13, 14), turbulent (Ref. A-4, 8, 12, 15 - 17), catalytic (Ref. A-8, 18) and shock tube (Ref. A-19) systems, both with and without fuel nitrogen (Ref. A-4 - 18), have been reported in the literature. Our purpose here is to establish the important species that contain fuel nitrogen and the effects of the combustion environment on these species.

During fuel-rich combustion, one of the first processes to occur is pyrolysis. Generally speaking, the pyrolysis of hydrocarbon fuels is complex, in some cases involving thirty distinct chemical reactions (Ref. A-19). The primary result of pyrolysis is that the nitrogen-containing ring structures in the fuel fracture and form free radicals such as NH, NH_2, NH_3 (usually denoted NH_i) and hydrocarbon fragments CH, CH_2, ... (or more generally CH_x) (Ref. A-20). These highly reactive species undergo further chemical reaction as the mixture passes through the reaction zone.

Typically, the major chemical species in combustion products are measured directly by sampling the products with a probe. The composition changes as the probe position moves further downstream. The major species include N_2, H_2O, CO_2, H_2, CO (Ref. A-15); the exact percentages varying with combustion conditions and fuel type. Pollutant related species generally occur in low concentration ($< 1\%$), but are important nonetheless. The species usually measured include NO, NO_2, HCN, various hydrocarbons and HN_3 (Ref. A-4 - 7, 9 - 12, 14 - 18).

In the literature dealing with pollutant formation during the rich burning of hydrocarbon fuels (with and without fuel nitrogen), the main components of interest are NO, NH_3, and HCN (Ref. A-4 - 7, 9 - 12, 14 - 21). These species play an integral role in NO_x formation from fuel-bound nitrogen and have been observed under all types of rich-combustion conditions (diffusion and premixed burning, laminar and turbulent flow, etc.). The exact chemical kinetic steps involved in the formation and destruction of NO, NH_3, HCN, etc. are still a matter of controversy, but it is clear that the kinetics are complicated (Ref. A-5 - 17, 21, 22). Published studies routinely include 15 species and 15 to 20 reactions; in one extreme case, 28 species and 120 reactions (Ref. A-8, 16, 17). Because of the existing uncertainty regarding the theoretical formation of pollutant-related species, we will focus our attention on the results of experimental studies in this discussion of prior work. By looking at the general trends of reported experimental work we can develop a rational strategy to minimize NO_x emissions.

We begin by examining NO, an important pollutant specie. In the reaction zone where temperatures are highest, NO is rapidly formed. Not surprisingly then, in flames where the temperature is the highest (i.e., around stoichiometric equivalence ratio), much NO is formed (Ref. A-23). For hydrocarbon fuels without fuel nitrogen, this behavior is well documented; as ϕ increases to ~1, NO increases and, for $\phi > 1$, NO decreases, becoming quite low beyond $\phi > 1.6$ (Ref. A-4 - 6, 9 - 12, 15 - 18). For fuels containing fuel nitrogen, the general trend is the same but the peak at $\phi = 1$ is very broad extending from $\phi = 0.8$ to 1.4. However, beyond $\phi = 1.6$, the NO formed is again very small, typically < 50 ppm. This behavior has been noted under widely varying combustion conditions from laminar premixed flames to turbulent diffusion flames. Suffice it to say that for hydrocarbon fuels with and without fuel nitrogen, burning at equivalence ratios richer than 1.6 is an effective way to suppress NO formation.

NO production also varies with residence time at a fixed equivalence ratio. The concentration of NO increases rapidly in the immediate

post flame zone, typically on a time scale of τ 2-6 ms (Ref. A-5, 6, 9 - 11, 13, 14, 16, 17), perhaps decreasing slightly for τ > 10-12 ms. These time scales were observed for laminar flat flame burners; for turbulent burners the NO concentration behavior is qualitatively the same, but with these burners it is difficult to make exact estimates of residence time. The principal feature is that after some time in the post flame zone, the NO concentration stays approximately constant or slowly decreases.

The next most important pollutant-related chemical specie is HCN. For hydrocarbon fuels (with and without fuel nitrogen), the formation of HCN is definitely favored as ϕ increases to ~ 1.7-1.8. For ϕ > 1.8 there is little data, and what data exists indicates that HCN formation falls off, becoming very low (i.e., < 25 ppm) around ϕ ~ 2 (Ref. A-5, 9, 14, 16 - 18).

The production of HCN as a function of residence time shows a distinctly different behavior than that of NO. Peak concentrations of HCN (which are comparable to or greater than those of NO) occur quickly in the post flame zone. These times are usually shorter than the time required for NO to peak. Further downstream, as residence time increases, the HCN disappears rapidly, falling to 1/3 to 1/4 of its peak value after ~10-12 ms. Presumably, the HCN is being converted to molecular nitrogen since the NO concentration decays very slowly with increased residence time. The same general behavior is noted for fuels with and without fuel nitrogen (Ref. A-5, 9, 14, 16, 17).

The final nitrogen-containing species of major importance is ammonia, NH_3, but there is comparatively less data on NH_3 than on HCN and NO. As with HCN, ammonia concentrations increase with ϕ up to a value of ~1.8 (Ref. A-9, 14, 19). There is little data available for ϕ > 1.8.

Ammonia concentration variation with residence time is similar to that of HCN. Peak concentrations of NH_3 occur in the immediate post flame zone. As residence time increases, the ammonia concentration drops (Ref. A-6, 9, 14, 16, 17).

Several calculations have been performed showing that, for hydrocarbon fuels containing fuel nitrogen, there is a strong minimum in the production of nitrogen-containing species (the sum of NO + NH_3 + HCN) in the equivalence ratio range 1.3 to 1.5 (Ref. 8). It has been claimed that this equivalence ratio range is the proper one for first stage burning since the sum of nitrogen-containing species is theoretically a minimum. The arguments against such a strategy are equally strong. First, the calculation is based on thermodynamic equilibrium, which is not usually attained in combustors with short residence times. Second, this strong minimum is usually not observed experimentally (Ref. A-4, 8, 14). Indeed, on flat flame and turbulent burners, there is experimental evidence that the sum of nitrogen compounds is reduced as ϕ approaches 2.0 (Ref. A-4). Third, for the range of equivalence ratios, 1.3-1.5, the nitrogen containing species are mostly NO with little HCN and NH_3. It is an experimental fact that NO persists in the post flame zone with-

out undergoing further reaction to molecular nitrogen. By burning at higher equivalence ratios in the first stage, the fuel nitrogen forms mostly HCN and NH_3 and little NO. Both HCN and NH_3 are known to decay in the post flame zone, thus reducing the concentration of fuel nitrogen-containing species passed to the second stage of combustion.

To summarize this section, we have examined the formation of pollutant-related species containing fuel nitrogen. The production of NO, HCN and HN_3 is clearly a function of both equivalence ratio and residence time. As the equivalence ratio is increased past $\phi \sim 1.7-1.8$, the production of nitrogen-containing compounds (NO, HCN and NH_3) falls off dramatically. Furthermore, as residence time in the post flame zone increases, HCN and NH_3 decay while NO stays approximately constant or decays slightly. Thermodynamic calculations suggest that the sum of all nitrogen-containing species is minimized at equivalence ratios in the range of 1.3 to 1.5. However, the experimental evidence of this minimum is not convincing. In the next section, we will consider the further oxidation of the first-stage combustion products.

D.   SECOND-STAGE LEAN COMBUSTION

At the end of first-stage combustion, the hydrocarbon fuel and air mixture originally present has been converted to a gaseous mixture containing H_2, CO, N_2, H_2O, CO_2, and small amounts of pollutant-related species, NO, HCN, and NH_3. This mixture must now be diluted with additional combustion air and burned. The NO_x production in the second stage results from thermal fixation of the nitrogen in the final combustion air as well as any conversion of NO, HCN and NH_3. For the fuels Jet A, JP5 and $H_2/CO/N_2$ mixtures (with no fuel nitrogen), it has been shown in this report and in Ref. A-24 that very low levels of NO_x can be achieved under lean burning conditions by thorough premixing of the fuel and the combustion air.

The conversion of fuel-produced nitrogen species (NO, NH_3, HCN) to NO_x is not as clear cut. There is little data showing NO_x yields for hydrocarbon fuels doped with NO, NH_3 and HCN at low equivalence ratios ($\phi < 0.5$). The available data shows that at $\phi = 0.6$, 19% of the nitrogen in the fuel appears as NO_x for a $H_2/CO/CH_4$/inerts mixture doped with NH_3 (Ref. A-12). In another study, it was reported that NO has the highest conversion yields (over 70%), followed by HCN (65%) and NH_3 (35%) (Ref. A-8). While this data is hardly conclusive, it suggests that since HCN and NH_3 have the lower conversion yields, the nitrogen intermediates should be biased towards HCN and NH_3 and away from NO. This indicates that the first stage combustion should be as rich as possible. One thing is clear, yields are very sensitive to the equivalence ratio in the first and second stage. At this time, an appropriate data base does not yet exist to determine the proper second stage equivalence ratio so as to minimize overall exhaust pollutant emission for a given first stage equivalence ratio.

REFERENCES

A-1. Pillsbury, P. W., et al., "Fuel Effects in Recent Combustion Turbine Burner Tests of Six Coal Liquids." Paper #79-GT-137 presented at the ASME Gas Turbine Conference & Solar Energy Conference, San Diego, California, March 12-15, 1979.

A-2. Hammond, D. C., Jr., "Operation of a GT-225 Diffusion Flame Combustor on Alternate Fuels: Performance Durability and Emissions." Paper #79-G-138 presented at the ASME Gas Turbine Conference & Solar Energy Conference, San Diego, California, March 12-15, 1979.

A-3. Moses, C. A. and Naegeli, D. W., "Fuel Property Effects or Combustor Performance," Paper #79-GT-178 presented at the ASME Gas Turbine Conference & Solar Energy Conference, San Diego, California, March 12-15, 1979.

A-4. Yamagishi, K., et al., 15th Symposium (Int'l.) on Combustion, The Combustion Institute, Pittsburgh, PA, 1975, p. 1157.

A-5. Bachmaier, F., Eberius, K. H., and Just, T., Combustion Science and Technology, Vol. 7, pp. 77-84, 1973.

A-6. Fenimore, C. P., and Jones, G. W., J. Physical Chemistry, Vol. 65, p. 198, 1961.

A-7. Fenimore, C. P., Combustion and Flame, Vol. 19, p. 189, 1972.

A-8. Folsom, B. A., Courtney, C. W., and Heap, M. P., "The Effects of LBG Composition and Combustor Characteristics on Fuel NO_x Formation," Paper #79-GT-185 presented at the ASME Gas Turbine Conference & Solar Energy Conference, San Diego, CA, March 12-15, 1979.

A-9. Haynes, B. S., Iverach, D., and Kirov, N. Y., 15th Symposium (Int'l.) on Combustion, The Combustion Institute, Pittsburgh, PA, 1975, p. 1103.

A-10. Iverach, F., Basden, K. S., and Kirov, N. Y., 14th Symposium (Int'l.) on Combustion, The Combustion Institute, Pittsburgh, PA, 1973, p. 767.

A-11. Iverach, D., Kirov, N. Y., and Haynes, B. S., Combustion Science and Technology, Vol. 8, p. 159, 1973.

A-12. Martin, F. J., and Dederick, P. K., 16th Symposium (Int'l.) on Combustion, The Combustion Institute, Pittsburgh, PA, 1977, p.191.

A-13. Merryman, E. L., and Levy, A., 15th Symposium (Int'l.) on Combustion, The Combustion Institute, Pittsburgh, PA, 1973, p. 1073.

A-14. Morley, C., Combustion and Flame, Vol. 27, pp. 189, 204, 1976.

A-15. Fenimore, C. P., 16th Symposium (Int'l.) on Combustion, The Combustion Institute, Pittsburgh, PA, 1977, p. 1065.

A-16. Takagi, T. et al., 16th Symposium (Int'l.) on Combustion, The Combustion Institute, Pittsburgh, PA, 1977, p. 181.

A-17. Takagi, T. et al., Combustion and Flame, Vol. 35, pp. 17-25, 1979.

A-18. Krill, W. V., Kesserling, J. P., and Chu, E. K., "Catalytic Combustion for Gas Turbine Applications," Paper #79-GT-188 presented at the ASME Gas Turbine Conference & Solar Energy Conference, San Diego, CA, March 12-15, 1979.

A-19. Miller, D. L. et al., "The High Temperature Thermal Decomposition of Methanol," Paper #WSS 79-15 presented at The Western States Section/The Combustion Institute Meeting, Provo, Utah, April 23-24, 1979.

A-20. Appleton, J. P., and Heywood, J. B., 14th Symposium (Int'l.) on Combustion, The Combustion Institute, Pittsburgh, PA, 1973, p.777.

A-21. De Soete, G. G., 15th Symposium (Int'l.) on Combustion, The Combustion Institute, Pittsburgh, PA, 1975, p. 1093.

A-22. Flagan, R. C., Galant, S., and Appleton, J. P., Combustion and Flame, Vol. 22, p. 299-311, 1974.

A-23. Nelson, H. F., AIAA Journal Vol. 14, No. 9, p. 1177-1182, 1976.

A-24. Semerjian, H., and Vranos, A., 16th Symposium (Int'l.) on Combustion, The Combustion Institute, Pittsburgh, PA, 1977, p. 169.

APPENDIX B

DESCRIPTION OF TWO-STAGE COMBUSTOR

A. INTRODUCTION

A precombustion stage and a final-stage premix section designed for integration with the water-cooled inlet, combustion chamber and exhaust nozzle components of the MOD 2M combustor described in Section III A of this report was constructed in preparation for two-stage combustion experiments. While these experiments have yet to be conducted, a brief description of the baseline apparatus will be given here. Since significant aspects of two-stage combustion are controlled by the combustor hardware, e.g., preheating, premixing, flame stabilization, and reaction volume, it is expected that design iterations on the baseline apparatus will be required in order to optimize its operation.

A schematic of the baseline apparatus is shown in Fig. B-1, a photographic view of the installation in the burner housing with the housing flange open is shown in Fig. B-2, and a photograph of the assembled precombustion stage and the second stage premix section is shown in Fig. B-3. Table B-1 lists the nominal design conditions.

Air from the burner housing plenum enters the combustor assembly at the two locations shown in Fig. B-1, the air split being controlled by the position of a remotely operated rotary damper (visible in Figs. B-2 and B-3) incorporated at the inlet assembly for the second stage. Air flowrate to the first stage is measured with a venturi meter. Total air flowrate to the plenum is also measured, therefore air to the second stage is determined as the difference between total and first stage flows.

Fuel is fed to the two stages from independently controlled flow circuits located outside of the burner housing. Each flow is measured by a turbine flowmeter. The fuel is not heated prior to entering the housing.

Ignition is provided by independently controlled torch ignitors (Air/H_2) located as shown in Fig. B-1 and B-3. First stage product gases, rapidly quenched and premixed with final stage air and additional fuel (in some modes of operation), are burned to completion in the combustion chamber of the second stage.

B. FIRST STAGE

The first stage was designed to regeneratively heat the already preheated air from the plenum, heat the liquid fuel for flash vaporization during injection, and to thoroughly premix the fuel and air prior to the fuel-rich reaction in the first stage combustion chamber. A disassembled view of the precombustor is shown in Fig. B-4.
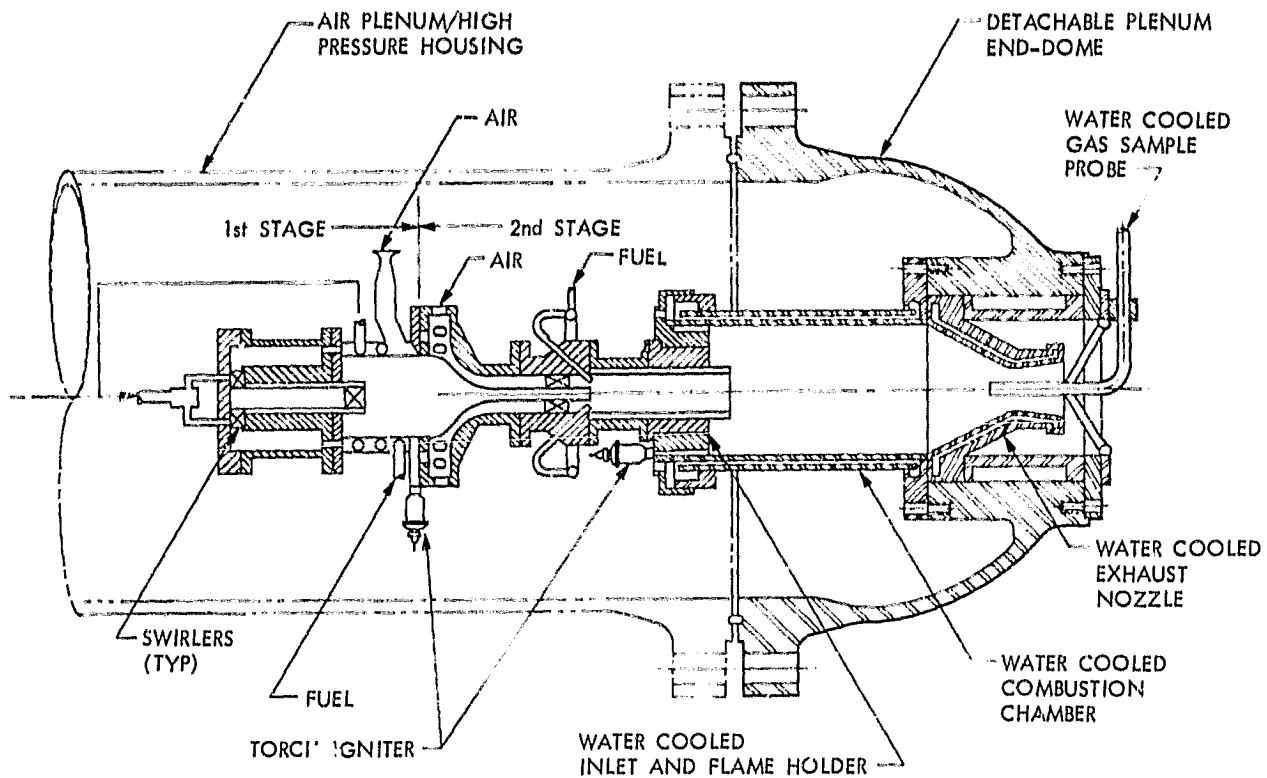
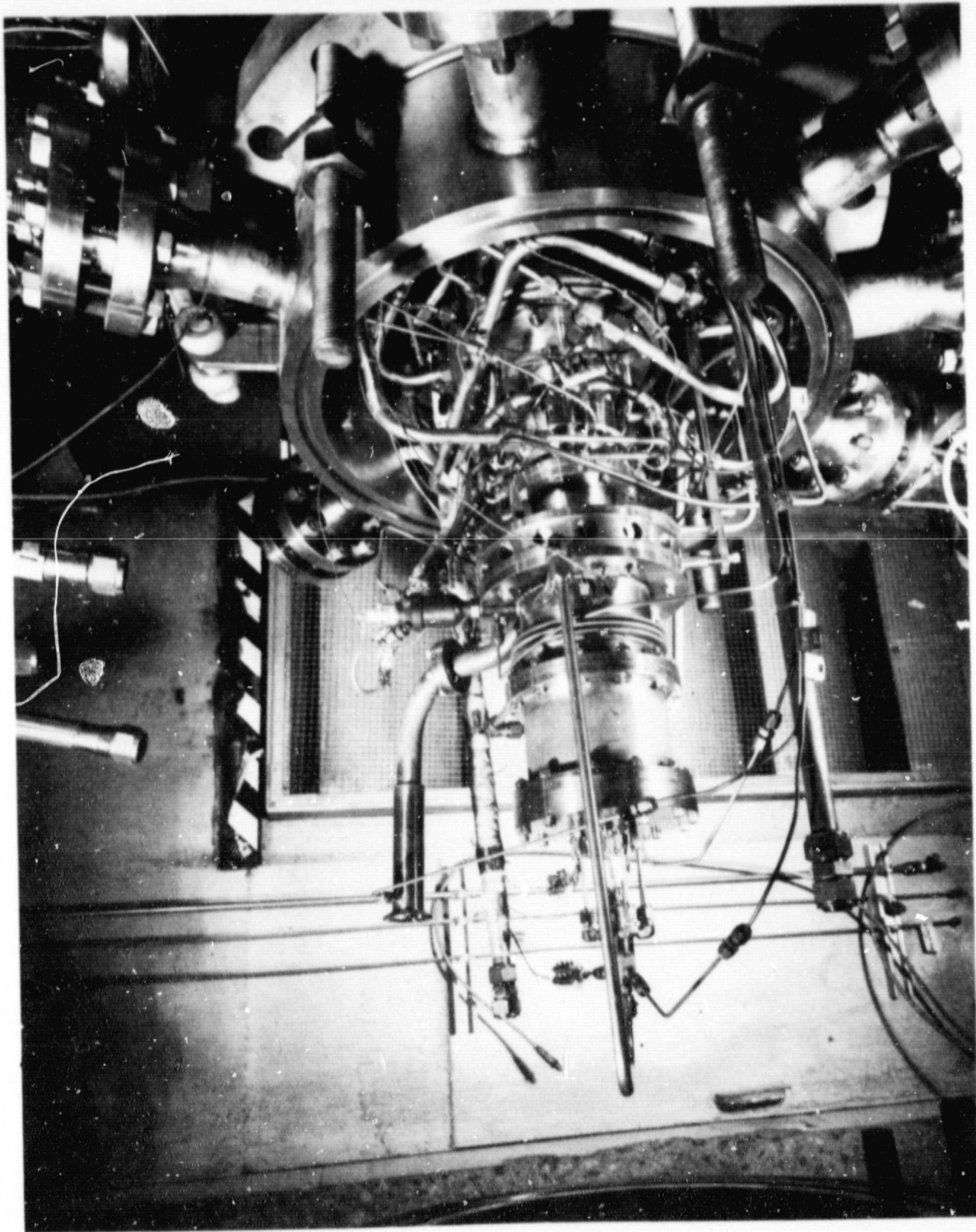Figure B-1. Two-stage research combustor installed in burner housing.

Figure B-2. Photographic view of two-stage combustor with burner-housing flange open.
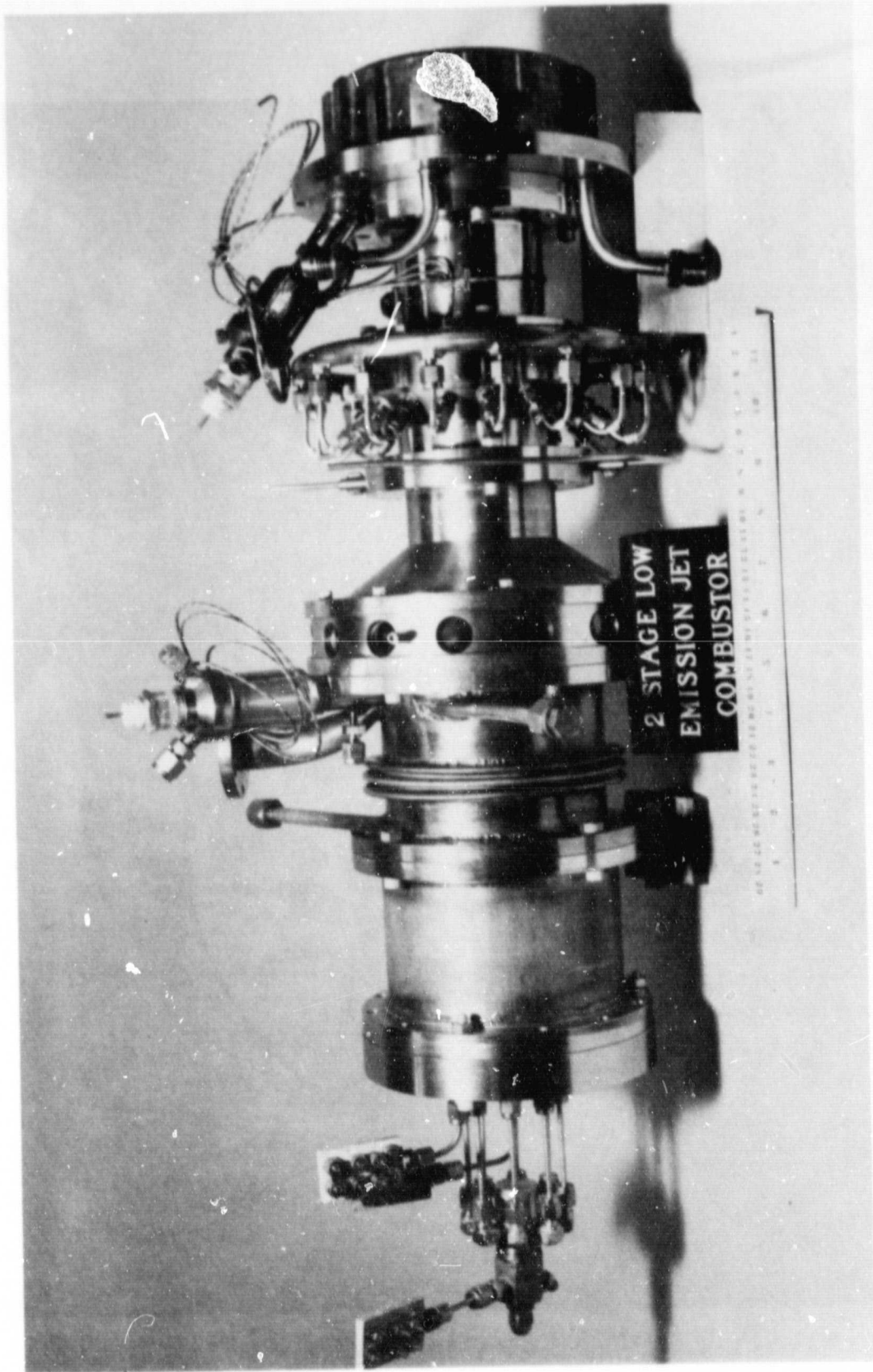
B-3

Figure B-3. Photograph of precombustion stage assembly and premix section assembly.

Table B-1. Design conditions for a two-stage research combustor based on $\phi_0 = 0.50$ and $\phi_g = 2.85$.

|	Operating Condition	
Design Parameter	Cruise	Takeoff
Overall combustor		
Air total pressure (plenum)	1.18 MPa (11.6 atm)	3.04 MPa (30 atm)
Air total temperature (plenum)	728 K (850 F)	811 K (1000 F)
Equivalence ratio (ϕ_0) range	0.30-0.70	0.31-0.70
Air flowrate	1.57 kg/s (3.46 lbm/s)	4.00 kg/s (8.81) lbm/s
Fuel flowrate	0.53 kg/s (0.117) lbm/s	0.135 kg/s (0.298 lbm/s)
Precombustion stage		
Regenerative preheat temperature	811 K (1000 F)	922 K (1200 F)
Equivalence ratio (ϕ_g)	2.85 (maximum)	2.85 (maximum)
Air flowrate		
10 air split	0.157 kg/s (0.346 lbm/s)	0.400 kg/s (0.881 lbm/s)
All fuel through first stage	0.277 kg/s (0.610 lbm/s)	0.700 kg/s (1.54 lbm/s)
Fuel flowrate		
10 air split	0.030 kg/s (0.067 lbm/s)	0.077 kg/s (0.170 lbm/s)
All fuel through first stage	0.053 kg/s (0.117) lbm/s	0.135 kg/s (0.298 lbm/s)
Premix residence time	2-4 ms	2-4 ms
Chamber residence time (no recirculation)	5-9 ms	5-9 ms
Chamber reference velocity	4.6-7.6 m/s (15-25 ft/s)	4.9-8.5 m/s (16-28 ft/s)
Product gas temperature	1422 K (2100 F)	1422 K (2100 F)
Product exit velocity	91-161 m/s (300-530 ft/s)	88-154 m/s (290-505 ft/s)
Premix swirl number	0.7	0.7
Flameholder swirl number	0.7	0.7
Final stage		
Air flowrate		
10 air split	1.41 kg/s (3.11 lbm/s)	3.60 kg/s (7.93 lbm/s)
All fuel through first stage	1.29 kg/s (2.85 lbm/s)	3.30 kg/s (7 27 lbm/s)
Fuel flowrate		
10 air split	0.023 kg/s (0.050 lbm/s)	0.058 kg/s (0.128 lbm/s)
All fuel through first stage	0	0
Premix temperature	849-927 K (1068-1208 F)	17-986 K (1191-1315 F)
Premix residence time	1 ms	1 ms
Premix axial velocity	162 m/s (532 ft/s)	168 m/s (551 ft/s)
Chamber residence time (no recirculation)	6 ms	5 ms
Chamber reference velocity	17.4 m/s (57 ft/s)	18.3 m/s (60 ft/s)
Air swirl number	0.7	0.7
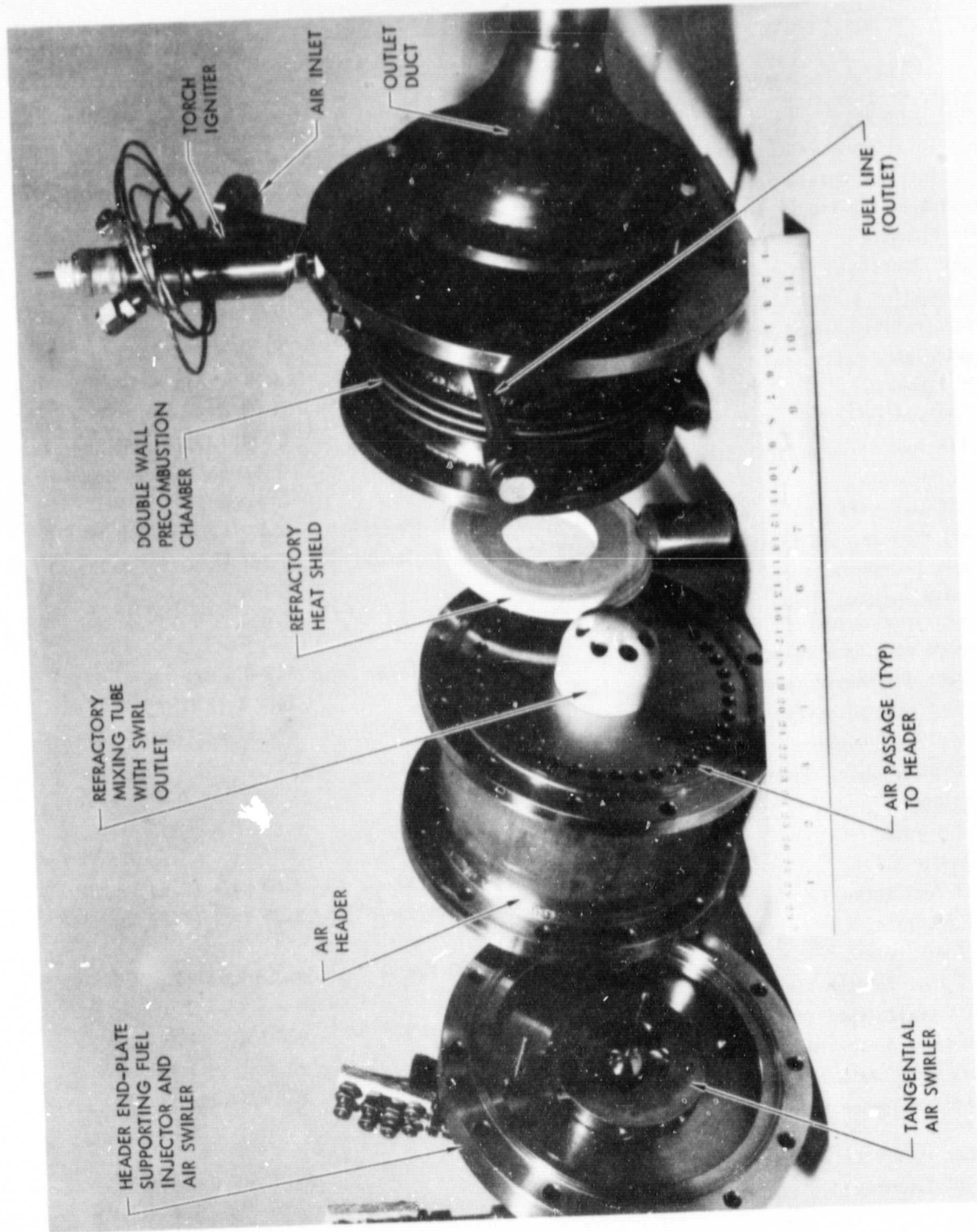
Figure B-4. Photograph of disassembled precombustion stage.

The air is heated during its passage along a helical passage formed by the double walls of the cylindrical chamber and the loosely coiled fuel line positioned between the walls (Fig. B-1). The heated air then passes to a header cavity from which it is injected into a refractory mixing tube [3.81-cm (1.5-in.) inside diameter x 11.43-cm (4.5-in.) inside length] through eight 7.62-mm (0.30-in.) diameter cylindrical passages, tangentially oriented to provide a flow swirl number in the mixing tube of approximately 0.7. Figure B-5 shows the swirler mounted on the header end-plate, and also the thermocouple probes for measuring the air temperature in the header cavity and the premix temperature in the mixing tube.

The unheated liquid fuel is supplied to the inlet end of the coiled-tube heat exchanger and the fuel is heated during its passage through the tube by the regeneratively heated air flowing toward the air header. The tube coil is not fastened to either of the walls of the combustion chamber except where it penetrates the outside wall, as apparent in Fig. B-3. Thus positive thermal contact with the hot chamber liner is avoided in order to reduce hot spots along the fuel tube. The 9.5-mm (0.375-in.) diameter, 0.51-mm (0.020-in.) wall thickness of the fuel tube provides a mean fuel velocity of 0.9 m/s (2.9 ft/s) through the tube.

After heating, the fuel is directed to a set of eight fuel injection tubes shown on the left-hand side of Fig. B-3. These tubes penetrate the header end-plate and the air swirler block with each tube-end flush with the inside wall of a swirler passage. A restrictor orifice located at the upstream end of each injection tube provides a pressure drop across which flash vaporization can occur. Thus, the initial fuel-air mixing occurs within the air swirler passages.

Further mixing takes place within the mixing tube, and finally the premixed reactants are injected into the precombustion chamber via the swirl generating outlet of the tube. A swirl number of about 0.7 is produced by the seven tangentially oriented cylindrical passages shown in Fig. B-4. These passages are 8.33 mm (0.328 in.) diameter and 25.4 mm (1.0 in.) long (by virtue of an extra thick refractory tube-end).

The swirl-flow of the reactant mixture provides a recirculation region in the first-stage combustion chamber, which stabilizes the partial oxidation reaction near the exit of the mixing tube. The intended appearance of this reaction zone is depicted in Fig. B-6 which shows a swirl-stabilized laboratory-scale burner with quartz walls operating at an equivalence ratio of ~2.0 (JP5/air). The fainter appearing flame at the exit (top) of the burner represents the final stage of combustion since it is the result of ingesting ambient air into the products of the fuel-rich reaction. Although the fuel-rich reaction appears to have a bright color, it was in fact a blue flame. The quartz tube produced a yellow coloration.

As shown in Table B-1 the precombustion residence time for the two-stage combustor is in the range of 5-9 ms, depending on actual first-stage throughput. This is about equivalent to the residence time
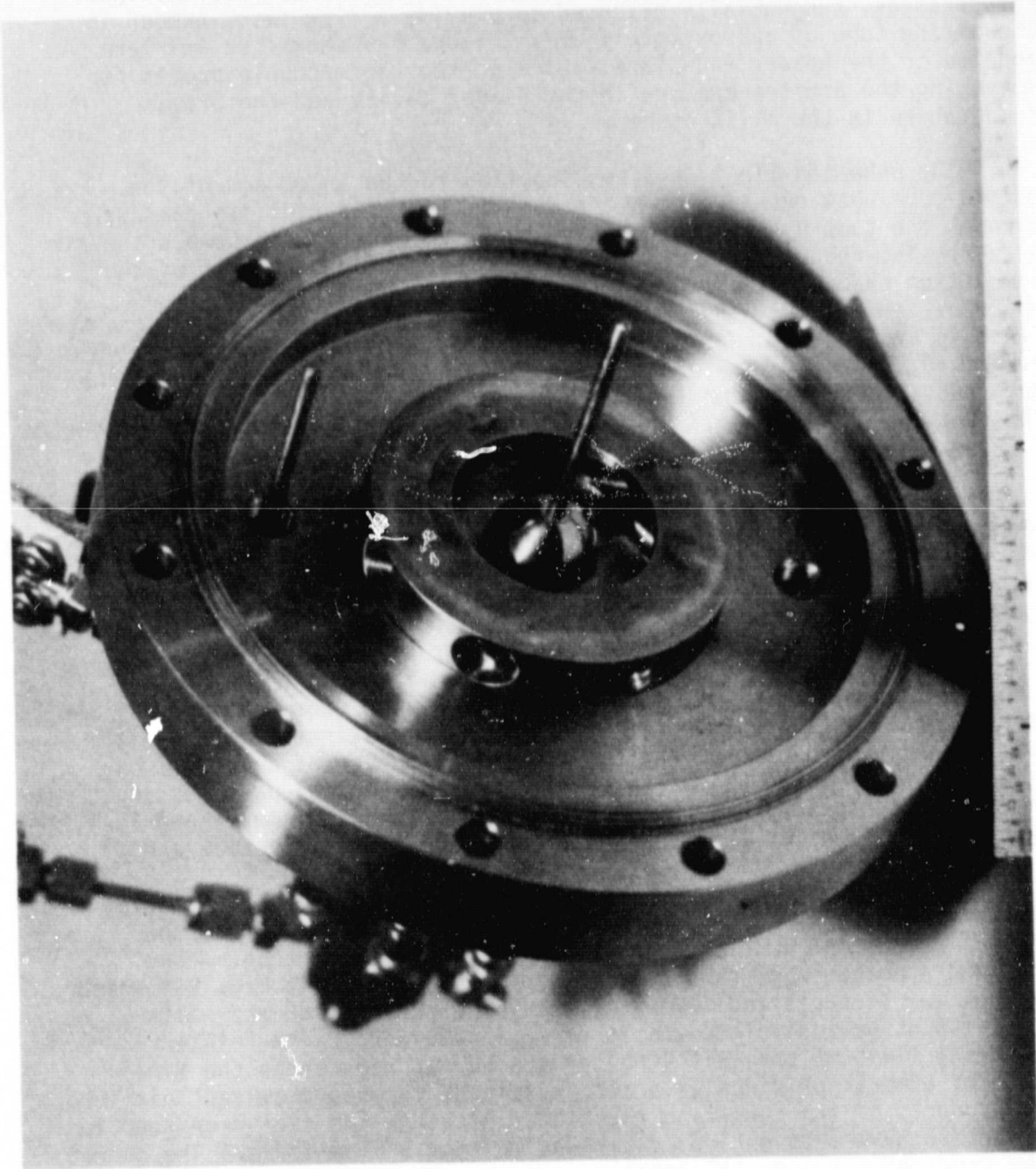
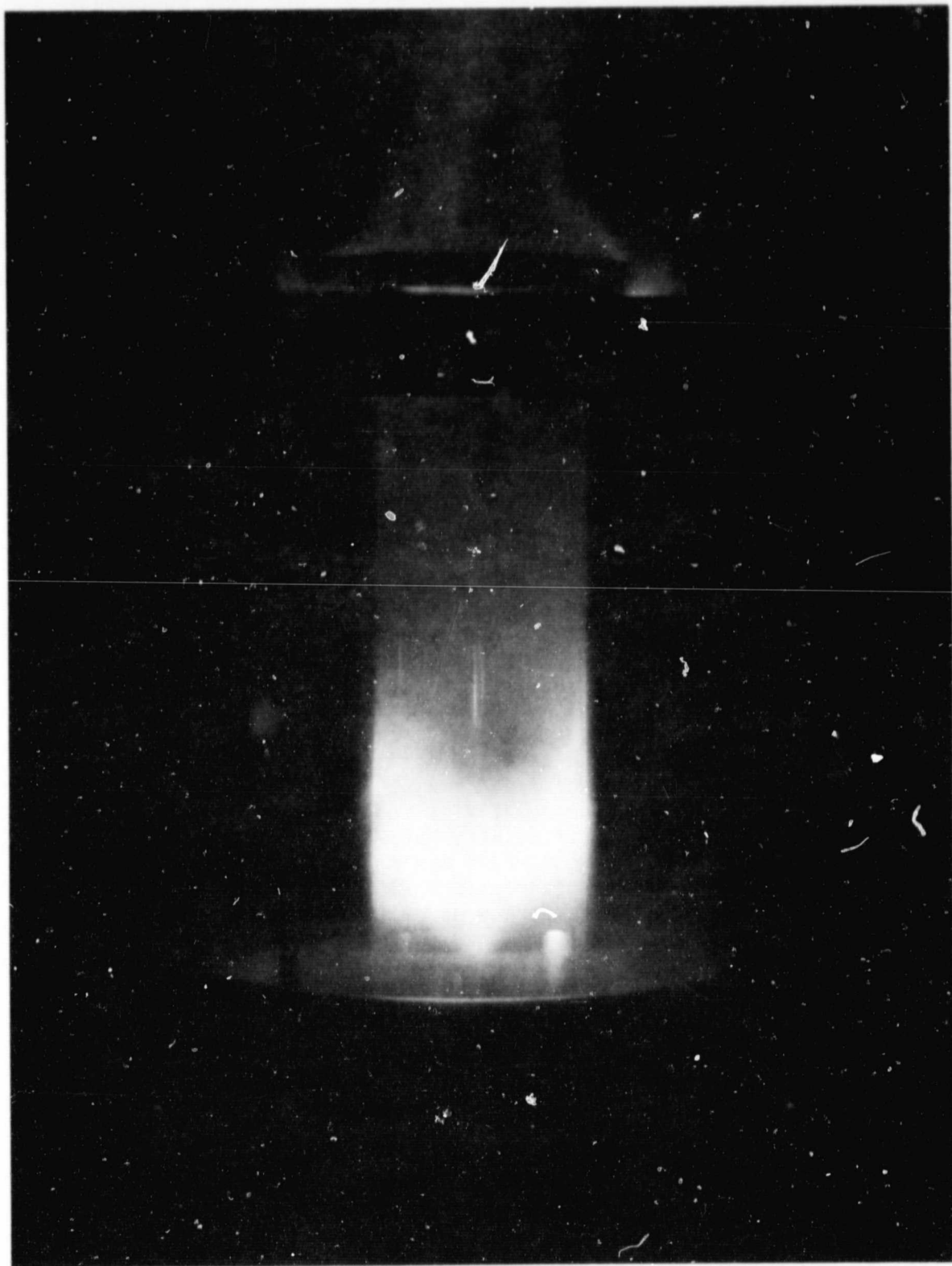Figure B-5. Photograph of air swirler for precombustion stage.

Figure B-6. Photograph of swirl stabilized precombustion
reaction in a laboratory scale burner with quartz walls.

for the final stage. This design condition was selected on the assumption that very fuel-rich reactions would exhibit the same combustion space rate as very fuel-lean reactions. Therefore, the first stage combustion volume was sized to be about 20% of the final stage volume since the maximum anticipated flow through the first stage was about 20% of the total flow.

C.   SECOND STAGE

The exit duct for the first stage shown schematically in Fig. B-1 is viewed at its exit plane in Fig. B-7. The flow from the centrally located, 3.66-cm (1.44-in.) diameter duct exits coaxially with the air flow for final combustion. The air flow has a swirl number of ~0.7 imparted by the swirler shown in Figs. B-1 and B-8, and is metered by the rotary damper valve (Fig. B-8) that controls the split of the air flow between the first and second stages.

When all the fuel is not processed through the first stage, the residual fuel is introduced into the second stage premixing section with low velocity through the sixteen injection tubes shown in Fig. B-7 and B-8.

All the major components of the second stage premixing section are shown and identified in Fig. B-8, including the portion of the inlet assembly for the combustion chamber that was adopted from the MOD 2M combustor. For the two-stage assembly the ellipsoidal bluff-body flameholder was removed, and the two-stage premixing tube (ceramic) was inserted through the central bore of the chamber inlet assembly. The annular flow area previously used was blocked by the mixing tube support and is not used for the two-stage combustor.

The strong swirl of the air flow as it enters the premixing section is intended to provide rapid mixing with the hot first stage product gas. And because the relatively cool air mass flow is always sufficient (by design) to provide very fuel-lean final equivalence ratios, it is expected that the rapid mixing and short (1 ms) residence time will promote quenching of reactions within the premixing section. Typical final stage premix temperatures calculated assuming no reaction are included in Table B-1.

Final combustion is stabilized by the swirl flow of the reactants as they exit the premix tube. Ignition of the final stage is provided by a torch ignitor. The 5-6 ms residence time of the final combustion volume appears to be adequate for efficient, low emission burning, as demonstrated by the results of experiments with a simulated product gas discussed in the main text of this report.
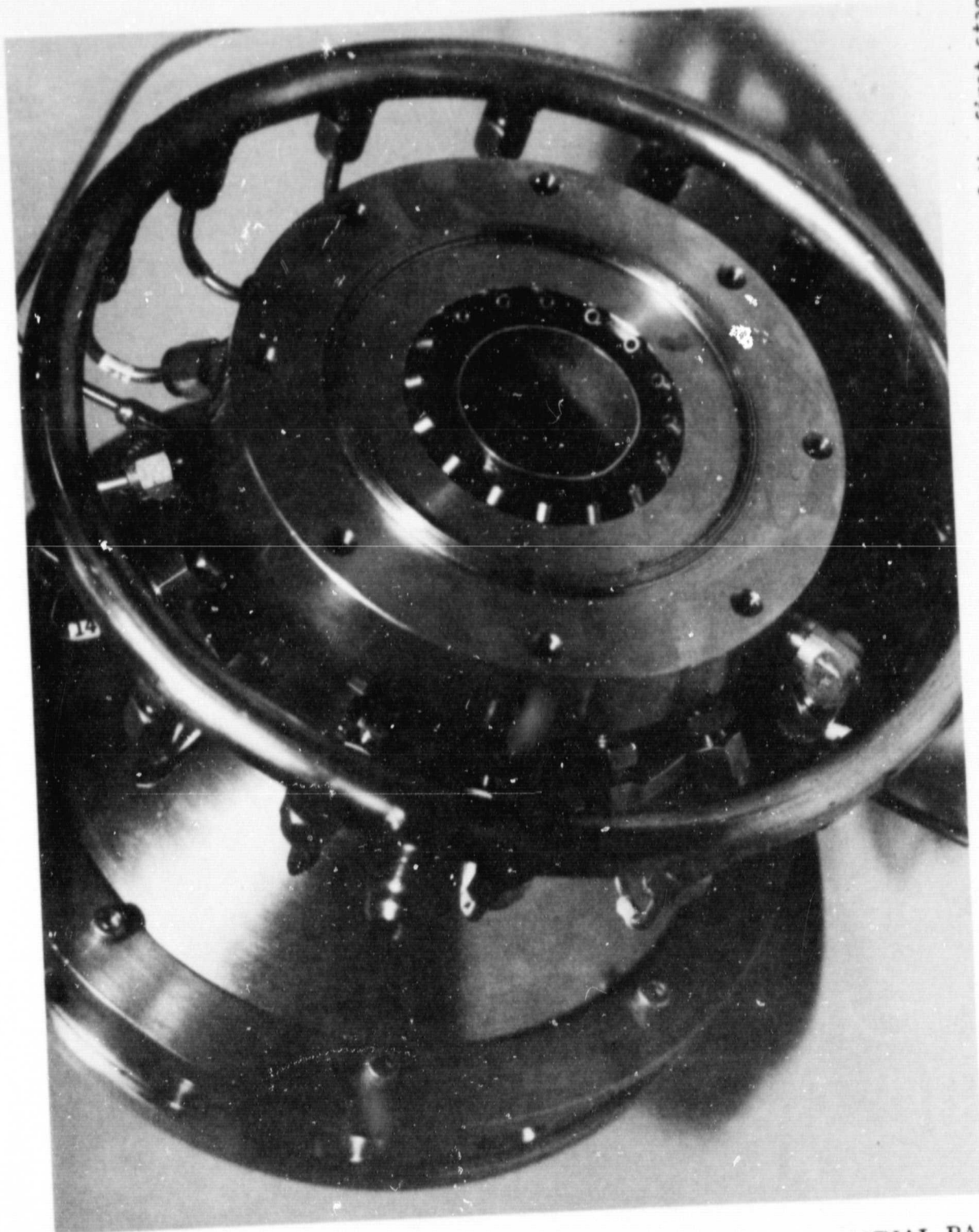
Figure B-7. Photograph of second stage mixing section at exit plane of the first stage.

INLET ASSEMBLY
TO SECOND
STAGE CHAMBER

TORCH IGNITER

REFRACTORY
MIXING TUBE

FUEL INJECTOR
ASSEMBLY

AIR INLET AND
ROTARY DAMPER
VALVE

AIR SWIRLER
BLADES

FIRST STAGE
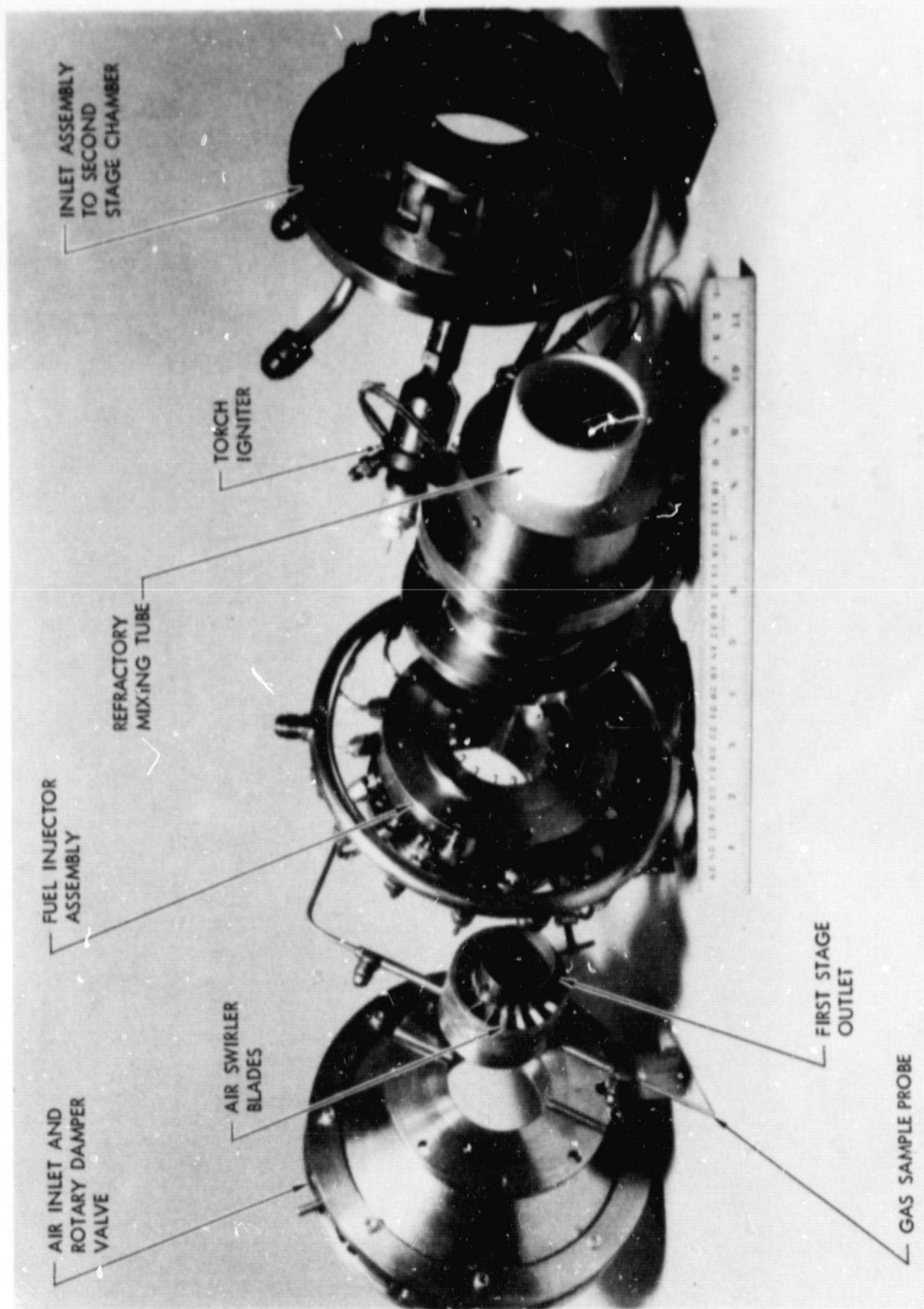OUTLET

GAS SAMPLE PROBE

Figure 3-8. Photograph of disassembled second stage premix section.

APPENDIX C

DERIVATIONS AND CALCULATION PROCEDURES

A.   DERIVATION OF TWO-STAGE LEAN-LIMIT EQUIVALENCE RATIO

For the purpose of estimating lean limit equivalence ratios (ϕ_{cL}) for two-stage systems it is convenient to consider the fuel to the second stage to be composed of a fuel-rich product stream from the first stage plus any raw fuel not processed through the first stage. Furthermore it is convenient to use the procedures outlined in Ref. C-1 for predicting the lean limit of any mixture of fuels from a knowledge of the lean limits for the individual fuels.

In Ref. C-2 it was shown that the Le Chatelier prediction formula described in Ref. C-1 could be expressed in terms of fuel/air mass ratio as

$$R_{LM} = \frac{\alpha_L}{1 + \beta_L F} \tag{C-1}$$

where:

R_{LM} = mass ratio of total fuel mix-to-air in the second stage in a lean-limit mixture (fuel mix comprises product gas plus additional raw fuel).

α_L = mass ratio of jet fuel-to-air in a lean-limit mixture; a constant for a fixed jet fuel.

F = mass fraction of product gas in the total fuel mix in the second stage.

β_L = $\dfrac{\alpha_L}{\alpha_{Lg}}$ - 1; with α_{Lg} being analogous to α_L and estimated from

Ref. C-1, considering the product gas as a fuel entity whose composition is a function of the first stage equivalence ratio (ϕ_q) and the inlet air state conditions; a constant for a fixed product composition.

Now in order to be most useful in establishing lean limits for two-stage combustor operation on an operating map such as shown in Fig. 4 of the main text, it is necessary to convert Eq. (C-1) to an expression giving the lean-limit equivalence ratio for the final combustion reaction (ϕ_{cL}) as a function of fuel split ratio (S_f).

In order to accomplish this the following definitions are made, using nomenclature that is consistant with Fig. 3 and Section II.B. of the main text.

$$S_f = \frac{\dot{m}_{fg}}{\dot{m}_{ft}} = \frac{S_a R_g}{R_0}$$

$$S_a = \frac{\dot{m}_{ag}}{\dot{m}_{at}} = \frac{S_f R_0}{R_g}$$

$$X = \frac{\dot{m}_{ad}}{\dot{m}_{at}}$$

$$R_g = \frac{\dot{m}_{fg}}{\dot{m}_{ag}} = R_s \phi_g$$

$R_s =$ stoichiometric fuel-to-air mass ratio for jet fuel.

$$R_c = \frac{\dot{m}_{ft}}{\dot{m}_{ag} + \dot{m}_{ac}} = R_s \phi_c$$

$$R_0 = \frac{\dot{m}_{ft}}{\dot{m}_{ag} + \dot{m}_{ac} + \dot{m}_{ad}} = \frac{\dot{m}_{ft}}{\dot{m}_{at}} = R_c(1-X) = R_s \phi_0$$

From the definition of R_{LM} and F in Eq. (C-1):

$$R_{LM} = \frac{\dot{m}_{ag} + \dot{m}_{fg} + \dot{m}_{fc}}{\dot{m}_{ac}} \tag{C-2}$$

and

$$F = \frac{\dot{m}_{ag} + \dot{m}_{fg}}{\dot{m}_{ag} + \dot{m}_{fg} + \dot{m}_{fc}} \tag{C-3}$$

After considerable algebraic manipulation of Eqs. C-2 and C-3 and substitutions of the other quantities defined above:

$$R_{LM} = \frac{R_0(S_f + R_g)}{R_g(1 - X) - S_f R_0} = \frac{\alpha_L}{1 + \beta_L \left(\frac{S_{f(1 + R_g)}}{S_f + \beta_g} \right)} \tag{C-4}$$

C-2

Rearrangement of Eq. (C-4) and conversion to overall equivalence ratio gives:

$$\phi_{oL} = \frac{R_O}{R_S} = \frac{\alpha_L R_g (1 - X)}{R_S \{R_g + S_f[1 + \alpha_L + \beta_L(1 + R_g)]\}} \tag{C-5}$$

or, since $\phi_O = \phi_C (1 - X)$,

$$\phi_{cL} = \frac{\alpha_L R_g}{R_S \{R_g + S_f[1 + \alpha_L + \beta_L(1 + R_g)]\}} \tag{C-6}$$

The values for α_L and β_L used in this report are based on information from Ref. C-1. Jet fuel (JP5) was considered to be the same as kerosene for which the volumetric lean limit in air, expressed as a fraction of the fuel vapor in the lean limit mixture, is given as 0.007. This converts to a fuel-to-air mass ratio (α_L) of 0.0414 assuming the molecular weights of fuel and air are 170 and 28.965, respectively.

β_L was computed for both the equilibrium product gas at $\phi_g = 2.83$ and the simulated product gas and found to be essentially the same, as would be expected (see gas compositions listed in Table 1 of the main text). Table C-1 shows the method of calculation for the equilibrium composition case for which β_L is -0.6533. The inerts are arbitrarily paired with the combustibles as shown; however, switching them around makes very little difference. For comparison, the β_L computed for the simulant gas was -0.6570.

B.   CALCULATION OF EMISSION INDEX

The emission index is defined as:

$$EI_p = ppm_p \times \overline{M}_p \times \left(1 + \frac{\dot{m}_{at}}{\dot{m}_{ft}}\right) \times 10^{-3}$$

where:

ppm$_p$ = measured volumetric concentration in parts per million of pollutant p in dry gas sample.

$\overline{M}_p$ = ratio of molecular weights of pollutant p to exhaust gas, taken as:

$\overline{M}_{HC}$ = 0.5585 (expressed as CH_4).

$\overline{M}_{CO}$ = 0.9773.

$\overline{M}_{NOx}$ = 1.6056 (expressed as NO_2).

Table C-1. Calculation of β_L for two-stage combustion; with $\phi_g = 2.83$ (equilibrium composition case).

Combustibles, % Vol		Inerts % Vol.			Total (P)	Lean Limit (N)
		CO_2	N_2	H_2O		
H_2	22.7	0.25	25.45	0.4	48.80	9.0
CO	24.7	0.25	25.45	0.4	50.80	27.0
CH_4	0.4				0.4	5.3

Volume fraction of product gas in lean limit mixture with air (Ref. C-1)

$$= \frac{1}{\dfrac{P_1}{N_1} + \dfrac{P_2}{N_2} + \dfrac{P_3}{N_3}}$$

$$= \frac{1}{\dfrac{48.80}{9.0} + \dfrac{50.80}{27.0} + \dfrac{0.4}{5.3}} = 0.1355$$

Equivalent gas-to-air mass ratio (α_{Lg}) using molecular weight of product gas of 22.05

$$= \frac{22.05 \times 0.1355}{28.965 \,(1 - 0.1355)}$$

Therefore, $\beta_L = \dfrac{\alpha_L}{\alpha_{Lg}} - 1 = \dfrac{0.0414}{0.1193} - 1 = -0.6533$

$\dot{m}_{at}$ = total(1) mass flow rate of air to combustion system.

$\dot{m}_{ft}$ = total(2) mass flow rate of fuel to combustion system.

Notes:

(1)   For the simulated-gas experiments, $\dot{m}_{at} = \dot{m}_{ag} + \dot{m}_{ac}$ (no dilution air was used), $\dot{m}_{ac}$ being measured directly and $\dot{m}_{ag}$ being determined by the relationship:

$$\dot{m}_{ag} = \frac{\dot{m}_g}{1 + R_g} = 0.834 \ \dot{m}_g$$

where

$\dot{m}_g$ = total measured simulant gas flowrate.
R_g = 0.1927 (ϕ_g = 2.83 assumed constant).

(2)   For the simulated-gas experiments, $\dot{m}_{ft} = \dot{m}_{fg} + \dot{m}_{fc}$, $\dot{m}_{fc}$ being measured directly and $\dot{m}_{fg}$ being determined by the relationship:

$$\dot{m}_{fg} = \frac{R_g \dot{m}_g}{1 + R_g} = 0.1616 \ \dot{m}_g$$

For the hydrogen-enrichment experiments, $\dot{m}_{ft} = \dot{m}_{JP} + \dot{m}_{H_2}$, where $\dot{m}_{JP}$ and $\dot{m}_{H_2}$ were measured directly.

C.   CALCULATION OF OVERALL EQUIVALENCE RATIO

Overall equivalence ratio is defined as:

$$\phi_0 = \frac{\dot{m}_{ft}}{R_s \ \dot{m}_{at}} = \frac{\dot{m}_{ft}}{0.068 \ \dot{m}_{at}}$$

where $\dot{m}_{ft}$ and $\dot{m}_{at}$ were calculated as above for the simulated-gas experiments and R_s = stoichiometric fuel-to-air mass ratio for jet fuel (taken to be 0.068).

For the hydrogen enrichment experiments:

$$\phi_0 = \frac{1}{\dot{m}_{at}} \left(\frac{\dot{m}_{JP}}{R_{SJP}} + \frac{\dot{m}_{H_2}}{R_{SH_2}} \right)$$

C-5

where:

$R_{SJP} = 0.068$ as before.

R_{SH_2} = stoichiometric fuel-to-air mass ratio for hydrogen (taken as 0.029).

REFERENCES

C-1   Coward, H. F., and Jones, G. W., Limits of Flammability of Gases and Vapors, Bulletin 503, Bureau of Mines, Washington, D. C., 1952.

C-2   Clayton, R. M., Reduction of Gaseous Pollutant Emissions From Gas Turbine Combustors Using Hydrogen-Enriched Jet Fuel-A Progress Report, Technical Memorandum 33-790, Jet Propulsion Laboratory, Pasadena, CA, October 15, 1976.